Available online at www.sciencedirect.com
ScienceDirect
Materials and Design 28 (2007) 1096–1115
Materials & Design
www.elsevier.com/locate/matdes

A study of composite beam with shape memory alloy arbitrarily embedded under thermal and mechanical loadings

Yin Zhang, Ya-Pu Zhao *

State Key Laboratory of Nonlinear Mechanics (LNM), Institute of Mechanics, Chinese Academy of Sciences, Beijing 100080, People's Republic of China

Received 16 May 2005; accepted 3 February 2006
Available online 31 March 2006

Abstract

The constitutive relations and kinematic assumptions on the composite beam with shape memory alloy (SMA) arbitrarily embedded are discussed and the results related to the different kinematic assumptions are compared. As the approach of mechanics of materials is to study the composite beam with the SMA layer embedded, the kinematic assumption is vital. In this paper, we systematically study the kinematic assumptions influence on the composite beam deflection and vibration characteristics. Based on the different kinematic assumptions, the equations of equilibrium/motion are different. Here three widely used kinematic assumptions are presented and the equations of equilibrium/motion are derived accordingly. As the three kinematic assumptions change from the simple to the complex one, the governing equations evolve from the linear to the nonlinear ones. For the nonlinear equations of equilibrium, the numerical solution is obtained by using Galerkin discretization method and Newton–Rhapson iteration method. The analysis on the numerical difficulty of using Galerkin method on the post-buckling analysis is presented. For the post-buckling analysis, finite element method is applied to avoid the difficulty due to the singularity occurred in Galerkin method. The natural frequencies of the composite beam with the nonlinear governing equation, which are obtained by directly linearizing the equations and locally linearizing the equations around each equilibrium, are compared. The influences of the SMA layer thickness and the shift from neutral axis on the deflection, buckling and post-buckling are also investigated.

This paper presents a very general way to treat thermo-mechanical properties of the composite beam with SMA arbitrarily embedded. The governing equations for each kinematic assumption consist of a third order and a fourth order differential equation with a total of seven boundary conditions. Some previous studies on the SMA layer either ignore the thermal constraint effect or implicitly assume that the SMA is symmetrically embedded. The composite beam with the SMA layer asymmetrically embedded is studied here, in which symmetric embedding is a special case. Based on the different kinematic assumptions, the results are different depending on the deflection magnitude because of the nonlinear hardening effect due to the (large) deflection. And this difference is systematically compared for both the deflection and the natural frequencies. For simple kinematic assumption, the governing equations are linear and analytical solution is available. But as the deflection increases to the large magnitude, the simple kinematic assumption does not really reflect the structural deflection and the complex one must be used. During the systematic comparison of computational results due to the different kinematic assumptions, the application range of the simple kinematic assumption is also evaluated. Besides the equilibrium study of the composite laminate with SMA embedded, the buckling, post-buckling, free and forced vibrations of the composite beam with the different configurations are also studied and compared.

Keywords: Shape memory alloy; Composite beam; Constitutive relation; Kinematic assumption; Equilibrium; Buckling/post-buckling; Vibration; Natural frequency

1. Introduction

In 1965, shape memory alloys (NITINOL) derived from Nickel and Titanium were first patented by Buehler and Wiley [1] in Naval Ordnance Laboratory. Since then,

* Corresponding author. Tel.: +86 10 6265 8008; fax: +86 10 6256 1284.
E-mail address: yzhao@lnm.imech.ac.cn (Y.-P. Zhao).

0261-3069/$ - see front matter © 2006 Elsevier Ltd. All rights reserved.
doi:10.1016/j.matdes.2006.02.001

tremendous effort has been infused to the utilization and study of this smart material. Constitutive relations have been theoretically developed or experimentally studied by Tanaka [2,3], Liang, Rogers [4,5], Xue and Mei [6], Cross et al. [7] and Jackson et al. [8]. In Liang's model [4], the stress in shape memory alloy (SMA) consists of three parts mechanical stress, thermo-elastic stress and the stress due to phase transformations. Xue's model is a 2D model and in his model the thermo-elastic stress and the stress due to phase transformation are combined together to be called recovery stress. Turner [9] averages the recovery stress including both the thermo-elastic stress and the stress due to phase transformation over the temperature range to get the effective coefficient of thermal expansion (CTE). Turner's method is to use effective CTE to simplify SMA nonlinear stress–strain relation, which is caused by both temperature and phase transformation. Epps and Chandra [11] use Euler–Bernoulli beam theory and model the effect of SMA in the composite beam as an axial force or an elastic foundation. Compared with the model of the beam under an axial load, the elastic foundation model of Epps and Chandra [11] has less bending stiffness. When the temperature goes higher, the difference between these two models enlarges. This may be due to the re-distribution of the stress due to the constraint which is not included in their equation of motion [12]. Baz and Ro [10] give the finite element model, which combines heat transfer and dynamic response together.

All the models mentioned above have one thing in common: SMA is implicitly assumed to be symmetrically embedded or its effect is modeled as an axial force or an elastic foundation. For the symmetric composite beam in those models, the governing equation is a fourth order equation of the transverse displacement without considering the coupling of axial and transverse displacements. A more general form of governing equations is derived here. For the symmetric composite beam, the governing equation is a set of equations consisting of a fourth order equation and a second order equation, which considers the coupling effect of axial and transverse displacement. For the uncoupling case, which only has the governing equation for the transverse displacement, only four boundary conditions are needed. For the coupling case of the symmetric beam, six boundary conditions are needed to solve such set of equations (two for axial displacement and four for transverse displacement). While for the asymmetric composite beam, two third of the derivatives due to the asymmetry appear in each of the two coupled equations of equilibrium for the transverse and axial displacement. And for the symmetric composite beam, the coefficients of the two third derivatives due to the asymmetry are zero. Therefore, for the asymmetric case, seven boundary conditions are needed. Mathematically, asymmetry increases one order of the governing equations. Asymmetry also causes the numerical difficulty of solving the equations, which is also discussed in the paper. Another purpose of this paper is to evaluate both the analytical and computational difference due to the different kinematic assumptions.

The shape memory effect (SME) is extensively used in the structure for active vibration/structural acoustic control [13,14] and shape control [15]. SMA is usually embedded in a composite laminate for such control functions. Besides the equilibrium study, this paper also explores the other topics closely related to the structure such as buckling, post-buckling, free and forced vibrations. By analyzing the difference caused by the different modeling or computation methods, a very comprehensive study on the modeling analysis and computation of the composite beam with the SMA layer arbitrarily embedded is presented.

2. Model development and analysis

2.1. Neutral axis and constitutive relation of SMA

The schematic diagram of the beam and its cross-section are shown in Figs. 1 and 2. Fig. 1 shows the neutral axis and coordinates of the composite beam cross-section. Fig. 2 shows the dimensions of the different layers. The beam studied here is a pinned-pinned beam. The pinned-pinned beam can allow the beam to move back and forth but not up and down. The beam length and width are L and b, respectively. The SMA layer width is b_1. In Fig. 1, h_1, h_4 are the distances between the neutral axis and the lower, upper edges of the beam, respectively, h_2, h_3 are the distances between the neutral axis and lower edge of SMA layer, respectively. The beam is under an axial mechanical load of p. For the approach of mechanics of materials, the first step is to find the neutral axis of the composite structure. The neutral axis is dependent on the configuration of the different layers and their elastic properties. For the cross-section of homogeneous material, the neutral axis is the centroidal axis [16]. For a composite beam with different material layers, the method of calculating the neutral axis is to convert different material properties inside the composite laminate into a "stressfully equivalent" homogeneous material [17,18]. By using the

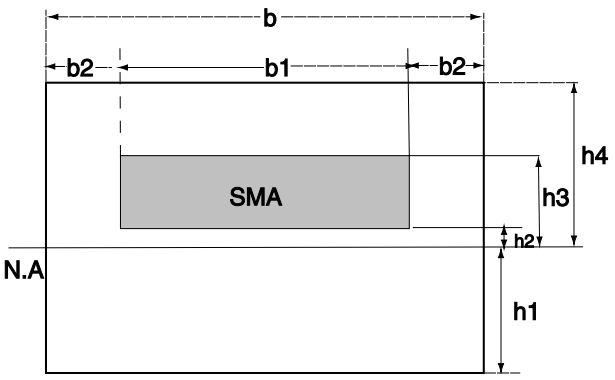

Fig. 1. Cross-section of a composite beam with the SMA layer embedded and the definitions of h_is ($i = 1, 2, 3, 4$).

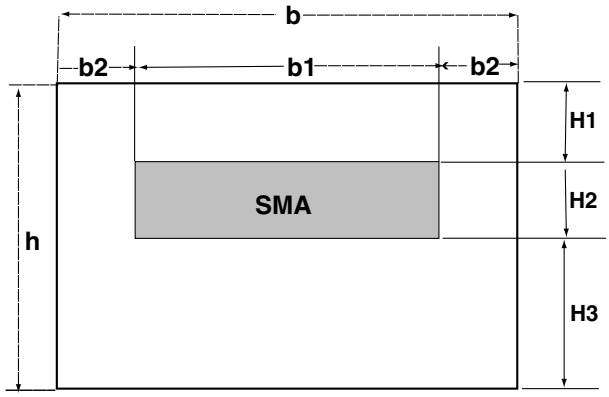

Fig. 2. The definition of H_is ($i = 1, 2, 3$).

formula of calculating the neutral axis of a composite cross-section [17], the neutral axis position, h_1, is calculated as

$$h_1 = \frac{\left(\frac{H_1}{2} + H_2 + H_3\right)H_1 b + \left(\frac{E_s}{E_c}b_1 + 2b_2\right)\left(H_3 + \frac{H_2}{2}\right)H_2 + \frac{H_3^2}{2}b}{(H_1 + H_3)b + \left(\frac{E_s}{E_c}b_1 + 2b_2\right)H_2}. \tag{1}$$

where H_is ($i = 1,2,3$) are the quantities indicated in Fig. 2, E_s and E_c are Young's moduli of SMA and epoxy, respectively. For the two moduli, they are generally temperature dependent variables [19]. The stress–strain relation of SMA given by Liang and Rogers [4,11] is

$$(\sigma - \sigma_0) = E_s(\xi)(\epsilon - \epsilon_0) + \Theta(T - T_0) + \Omega(\xi - \xi_0). \tag{2}$$

where the terms with subscript 0 are the initial conditions of the beam, σ and ϵ are stress and strain, respectively, T is Celsius temperature and Θ is thermo-elastic coefficient [11], which can be expressed as $-E(\xi)\alpha_s$. Here α_s is the SMA coefficient of thermal expansion (CTE). The parameter ξ is the martensite volume fraction and defined as the volume of martensite divided by total volume of martensite and austensite. In Liang and Rogers's cosine model [4], the parameter ξ is different for the reverse (from martensite to austensite) and the forward (from austensite to martensite) transformations.

For the reverse transformation, the martensite volume fraction is

$$\xi = \frac{\xi_M}{2}\cos[a_A(T - A_s) + b_A\sigma] + 1, \tag{3}$$

where

$$a_A = \frac{\pi}{A_f - A_s}, \quad b_A = -\frac{a_A}{C_A}, \tag{4}$$

and

$$C_A = \left(\frac{dA_s}{d\sigma}\right)^{-1}. \tag{5}$$

For the forward transformation

$$\xi = \frac{1 - \xi_A}{2}\cos[a_M(T - M_f) + b_M\sigma] + \frac{(1 + \xi_A)}{2}, \tag{6}$$

where

$$a_M = \frac{\pi}{M_s - M_f}, \quad b_M = -\frac{a_M}{C_M}, \tag{7}$$

and

$$C_M = \left(\frac{dM_s}{d\sigma}\right)^{-1}. \tag{8}$$

Here A_f is austensite finish temperature, A_s is austensite start temperature. M_f is martensite finish temperature, M_s is martensite start temperature. These temperatures are experimentally determined.

In Xue and Mei's model [6], the stress–strain relation for SMA is:

$$\sigma_s = E_s\epsilon + \sigma_r \quad (T > T_{s1}, \text{SMA activated}), \tag{9}$$

and

$$\sigma_s = E_s(\epsilon - \alpha_s\Delta T) \quad (T < T_{s1}, \text{SMA inactivated}). \tag{10}$$

where T_{s1} is the temperature at which the SMA is activated. For the epoxy composite matrix, the following constitutive relation holds:

$$\sigma_c = E_c(\epsilon - \alpha_c\Delta T). \tag{11}$$

where α_s and α_c are CTEs of SMA and epoxy, respectively, ΔT is the beam temperature difference with the ambient environment. In Xue and Mei's model [6], the recovery stress includes both thermal stress and the stress due to phase transformation. While in most cases, as shown in Eq. (2) [4], the two different kinds of stress are differentiated. And it is worth pointing out that for both SMA and epoxy layer in Eqs. (9)–(11), there is only one strain variable ϵ. For the effect of one strain variable on the constraint due to the interlameller bonding, the discussion can be found in the referred paper [12].

2.2. Kinematic assumptions

As the neutral axis and the constitutive relations are presented in the above section, another important thing for modeling the composite beam is the kinematic assumption. Three kinematic assumptions for Euler–Bernoulli thin beam modeling are presented in this paper. The governing equations derived from the three kinematic assumptions are discussed. Before we give the kinematic assumptions and derive the governing equation, we define the following parameters first:

$$A = E_c bQ_1 + 2E_c b_2 R_1 + E_c bS_1 + E_s b_1 R_1,$$

$$B = \frac{1}{2}(E_c bQ_2 + 2E_c b_2 R_2 + E_c bS_2 + E_s b_1 R_2),$$

$$D = \frac{1}{2}(E_c bQ_3 + 2E_c b_2 R_3 + E_c bS_3 + E_s b_1 R_3),$$

and Q_i, R_i and S_i are defined as

$$Q_1 = h_1 - h_3, \quad R_1 = h_3 - h_2, \quad S_1 = h_2 - h_1,$$
$$Q_2 = h_1^2 - h_3^2, \quad R_2 = h_3^2 - h_2^2, \quad S_2 = h_2^2 - h_1^2,$$
$$Q_3 = \frac{2}{3}(h_1^3 - h_3^3), \quad R_3 = \frac{2}{3}(h_3^3 - h_2^3), \quad S_3 = \frac{2}{3}(h_2^3 - h_1^3).$$

Though they have the complex forms, A, B and D have the very specific physical meanings for the composite beam. From Fig. 1, it is not that difficult to conclude that A is the effective axial stiffness. A can be derived if each layer of the different materials is modeled as a spring and the springs are in a parallel configuration [6,12,18]. The physical meaning of B and D will be discussed later.

Kinematic assumption 1 [20] is expressed as:

$$\epsilon = \epsilon_s + \epsilon_b = \frac{p}{A} + u_x - y v_{xx}. \tag{12}$$

where u and v are the axial and the transverse displacements, respectively, ϵ_s is the strain due to the stretching of the axial load and ϵ_b is the strain due to the bending. For all the three kinematic assumptions presented in this paper, the bending strain is denned as $\epsilon_b = -y v_{xx}$. This bending strain is derived from the linear moment–curvature relationship [21] and it is sufficiently accurate even for the large deflection case as far as $I/SL^2 < 0.001$ (I, second moment of area; S, cross-section area; and L, beam length) [21,22].

Kinematic assumption 2 [20] is expressed as:

$$\epsilon = \epsilon_s + \epsilon_b = \frac{p}{A} + u_x + \frac{v_x^2}{2} - y v_{xx}. \tag{13}$$

Kinematic assumption 3 [21,22] is expressed as:

$$\epsilon = \epsilon_s + \epsilon_b = \frac{p}{A} + [(1+u_x)^2 + v_x^2]^{\frac{1}{2}} - 1 - y v_{xx}. \tag{14}$$

For the convenience of computation, the constitutive relation for SMA in Eqs. (9) and (10) is re-written in one as follows:

$$\sigma_s = E_s(\epsilon - \alpha_s \Delta T) + \sigma_p. \tag{15}$$

where σ_p is the stress due to phase transformation and is dependent on temperature, which matches $\Omega(\xi - \xi_0)$ term in the Liang's model [4]. σ_p is either computed by the complex formula by Liang [4] or in practice supplied by the experimental data. The stress in epoxy remains the same as that of Eq. (11).

2.3. Derivation of equations of equilibrium

The potential energy in the SMA layer, which contains both the stretching and the bending energies, is as follows:

$$U_s = \frac{1}{2}\int_0^L \int_{A_M} [E_s(\epsilon - \alpha_s \Delta T) + \sigma_p]\epsilon \, dA \, dx, \tag{16}$$

where A_M is the SMA cross-section area of the beam. The potential energy in the epoxy layers is

$$U_s = \frac{1}{2}\int_0^L \int_{A_c} [E_c(\epsilon - \alpha_c \Delta T)]\epsilon \, dA \, dx, \tag{17}$$

where A_c is the epoxy cross-section area of the beam.

By applying the principle of minimum potential energy (PMPE), i.e., $\delta(U_s + U_c) = 0$, and plugging the different ϵs of the different kinematic assumptions, the equations of equilibrium are obtained. For kinematic assumption 1, the equations of equilibrium are obtained in the following two forms:

$$B v_{xxx} - A u_{xx} = 0, \tag{18}$$

and

$$D v_{xxxx} - B u_{xxx} = 0. \tag{19}$$

The two equations of equilibrium are obtained by re-grouping the variables u and v after the variational operation and integration by parts. Let us first discuss what are the physical meanings for B and D. To the authors' knowledge, there is no name for B though it frequently appears in the composite structure analysis. From the expression of B given above, B is a parameter indicating the asymmetry of the composite beam cross-section. $B = 0$ is for symmetric cross-section. When $B = 0$, Eqs. (18) and (19) are two uncoupled ordinary differential equations, which is the scenario for many studies on composite beam with SMA embedded [11]. From its definition and Eq. (19), it is not that difficult to conclude that parameter D is the effective bending stiffness of the composite beam. For thin beam, D is much smaller than A; therefore, the axial displacement u is much smaller than v in the small deflection with the relatively low axial loading scenario. So in many studies of small deflection cases, u and its coupling contribution to the deflection are small and thus ignored. Clearly, here u and v are coupled by the asymmetry parameter B. For the symmetric case of $B = 0$, the axial displacement u and the transverse displacement v are coupled via the kinematic assumption of large deformation as those of kinematic assumptions 2 and 3 shown later. As it is noticed that in Eqs. (18) and (19), there is no term associated with the axial load p. In the buckling study of beam, p is shown in a fourth order governing equation as a second order term $p v_{xx}$. But this $p v_{xx}$ term is due to the $\frac{v_x^2}{2}$ term in the kinematic assumption of strain, which is included in kinematic assumption 2 but not in kinematic assumption 1. While it will be shown later that the axial load effect of p is actually included in the boundary conditions for kinematic assumption 1. The boundary conditions can also be derived during the derivation of governing equations by using PMPE. For the seven boundary conditions, we will have detailed discussion later in Section 3.

The two governing equations of equilibrium due to kinematic assumption 2 are

$$Bv_{xxx} - Au_{xx} = Av_x v_{xx} + B\left(v_x v_{xx}^2 + \frac{v_x^2 v_{xxx}}{2}\right) \tag{20}$$

and

$$Dv_{xxxx} - Bu_{xxx} - \left[(A - E_s b_1 R_1)\left(g_0 - \frac{\alpha_c \Delta T}{2}\right) + E_s b_1 R_1 \left(g_0 - \frac{\alpha_s \Delta T}{2}\right) + \frac{1}{2} b_1 R_1 \sigma_p\right] v_{xx} = A\left(u_{xx} v_x + u_x v_{xx} + \frac{3 v_x^2 v_{xx}}{2}\right). \tag{21}$$

Here we define g_0 as $g_0 = \frac{p}{A}$, which is the stretching strain due to the external mechanical load p. So compared with Eqs. (18) and (19), Eqs. (20) and (21) are much more complex. Before we continue to derive the governing equation for kinematic assumption 3, let us first make some simple comparison analysis for these two sets of governing equations. As it is noticed, the right side terms in Eqs. (20) and (21) are the nonlinear terms of $v_x v_{xx}, v_x v_{xx}^2, v_x^2 v_{xxx}$ and $u_{xx} v_x$ which are at least one order of magnitude smaller than those linear terms (v_{xxxx}, v_{xxx}, u_{xxx} and u_{xx}). If all the right side terms of Eqs. (20) and (21) are set to be zero for the approximation purpose, the difference of the two sets of equations is only reflected in the $[(A - E_s b_1 R_1)(g_0 - \frac{\alpha_c \Delta T}{2}) + E_s b_1 R_1 (g_0 - \frac{\alpha_s \Delta T}{2_2}) + \frac{1}{2} b_1 R_1 \sigma_p] v_{xx}$ term in Eq. (21). And this is due to the $\frac{v_x}{2}$ term in kinematic assumption 2. $(A - E_s b_1 R_1)(g_0 - \frac{\alpha_c \Delta T}{2}) + E_s b_1 R_1 (g_0 - \frac{\alpha_s \Delta TT}{2}) + \frac{1}{2} b_1 R_1 \sigma_p$ is the effective axial loading including the mechanical, thermal forces and the force due to the phase transformation.

The two equations of equilibrium for kinematic assumption 3 are the following:

$$Bv_{xxx} - Au_{xx} = \left[(A - E_s b_1 R_1)\left(1 - g_0 + \frac{\alpha_c \Delta T}{2}\right) + E_s b_1 R_1 \left(1 - g_0 + \frac{\alpha_s \Delta T}{2}\right) - \frac{1}{2} b_1 \sigma_p R_1\right] v_x v_{xx} + B\left(v_x v_{xx}^2 + \frac{v_x^2 v_{xxx}}{2}\right), \tag{22}$$

and

$$Dv_{xxxx} - Bu_{xxx} - \left[(A - E_s b_1 R_1)\left(g_0 - \frac{\alpha_c \Delta T}{2}\right) + E_s b_1 R_1 \left(g_0 - \frac{\alpha_s \Delta T}{2}\right) + \frac{1}{2} b_1 R_1 \sigma_p\right] v_{xx} = \left[(A - E_s b_1 R_1)\left(1 + \frac{\alpha_c \Delta T}{2} - g_0\right) + E_s b_1 R_1 \left(1 + \frac{\alpha_c \Delta T}{2} - g_0\right) + E_s b_1 R_1 \left(1 + \frac{\alpha_s \Delta T}{2} - g_0\right) - \frac{1}{2} b_1 R_1 \sigma_p\right] \times \left(u_{xx} v_x + u_x v_{xx} + \frac{3 v_x^2 v_{xx}}{2}\right). \tag{23}$$

The linear parts of equations of equilibrium for kinematic assumptions 2 and 3 are the same. The difference is in their nonlinear parts. By comparing the nonlinear parts, the conclusion can be made that without the thermo-elastic stress, the stress due to phase transformation and the mechanical load (p), kinematic assumptions 2 and 3 get the same equations of equilibrium. When these three stresses increase, the equations of kinematic assumptions 2 and 3 will enlarge their difference in the nonlinear terms. The difference enlarges as the loading or the deflection becomes larger, or say, the nonlinear effect due to the large loading or the deflection increases. The equations derived from kinematic assumption 1 are the same as these derived by Vinson and Sierakowski [23] if the hygrometric load, distributed stresses and moments are ignored in their equation. The load p is not shown in the equations of kinematic assumption 1, but appears in boundary conditions, which will be discussed later. The mechanical load p (associated with g_0) and other axial loadings (due to thermo-mechanical stress and phase transformation) are seen in both of the governing equation sets derived from kinematic assumptions 2 and 3. It should not be that difficult to conclude that the governing equations derived from kinematic assumption 1 are not accurately enough even for the linear small deflection analysis because the linear term associated with the axial loading is not shown in the governing equations.

In Xue, Mei [6] and Turner's [9] model, there is a 2D plate for the beam with the SMA layer embedded. Here the model is Euler–Bernoulli beam theory, which is actually an, 1D model. King [24] notices that for the "ideal" composite material, in which the fibers are inextensible, the inextensibility reduces the stiffness and the stiffness predicted by the "ideal" composite beam theory has less stiffness than that predicted by Timoshenko beam theory. However, the difference between the "ideal" composite beam theory and Timoshenko beam theory is relatively small [24]. Compared with Timoshenko beam theory, Euler–Bernoulli beam theory does not consider the shearing effect. In kinematic assumptions 1, 2 and 3, the strain is normal strain, shear strain is not included. The structural stiffness computed by Euler–Bernoulli beam theory is larger than that of Timoshenko beam theory. The applicability range of these two theories is dependent on aspect ratio of the thickness to the length of the beam. The rule of thumb is the following: Timoshenko beam theory is applied to the "thick" beam with the aspect ratio of the thickness to the length larger than 1/7. For the "thin" beam with the smaller aspect ratio, it is the applicability range of Euler–Bernoulli beam theory. Euler–Bernoulli beam theory is widely used to study the anisotropic composite structure [11,23]. This paper focuses only on the study on the kinematic assumptions influence on the computational results of Euler–Bernoulli beam. Among all these three kinematic assumptions, kinematic assumption 3 is the most accurate. Kinematic assumption 2 is actually an approximation of kinematic assumption 3. To show this, we give the following:

$$\epsilon = \frac{p}{A} + [(1 + u_x)^2 + v_x^2]^{\frac{1}{2}} - 1 - y v_{xx}$$
$$\approx \frac{p}{A} + 1 + u_x + \frac{v_x^2}{2} - 1 - y v_{xx} = \frac{p}{A} + u_x + \frac{v_x^2}{2} - y v_{xx}$$

2.4. Nondimensionalization of equations of equilibrium

In order to nondimensionalize, the following dimensionless numbers are introduced:

$$\zeta = \frac{x}{L}, \quad V = \frac{v}{L}, \quad U = \frac{u}{L}.$$

The dimensionless equations of Eqs. (22) and (23) are obtained as follows:

$$\beta V_{\zeta\zeta\zeta} - \alpha_1 U_{\zeta\zeta} = \eta V_\zeta V_{\zeta\zeta} + \beta\left(V_\zeta V_{\zeta\zeta}^2 + \frac{V_\zeta^2 V_{\zeta\zeta}}{2}\right), \tag{24}$$

and

$$V_{\zeta\zeta\zeta\zeta} - \beta U_{\zeta\zeta\zeta} - \alpha V_{\zeta\zeta} = \eta\left(U_{\zeta\zeta} V_\zeta + U_\zeta V_{\zeta\zeta} + \frac{3}{2} V_\zeta^2 V_{\zeta\zeta}\right). \tag{25}$$

Here α_1, α, β, and η are defined as

$$\alpha = \alpha_1\left(g_0 - \frac{\alpha_c \Delta T}{2}\right) + \alpha_2\left(g_0 - \frac{\alpha_s \Delta T}{2}\right) + \alpha_3,$$

with

$$\alpha_1 = \frac{AL^2}{D}, \quad \alpha_2 = \frac{2L^2 E_s b_1 R_1}{D}, \quad \alpha_3 = \frac{L^2 b_1 R_1 \sigma_p}{D},$$

and

$$\beta = \frac{BL}{D}, \quad \eta = -\alpha + \alpha_1 + \alpha_2.$$

The linear parts of Eqs. (24) and (25) are the following:

$$\beta V_{\zeta\zeta\zeta} - \alpha_1 U_{\zeta\zeta} = 0, \tag{26}$$

and

$$V_{\zeta\zeta\zeta\zeta} - \beta U_{\zeta\zeta\zeta} - \alpha V_{\zeta\zeta} = 0. \tag{27}$$

The nonlinear parts of Eqs. (24) and (25) are the higher order term. The two linear equations above, which include the axial force influence, are relatively accurate for the small deflection.

3. Solutions and results discussion for the equations of equilibrium

3.1. Analytical solutions of linear equations of equilibrium

The boundary conditions need to be given to derive analytical solutions of Eqs. (26) and (27). As for all the governing equation sets derived from the three kinematic assumptions, the highest order of the derivative in one equation is 4th order, the other highest in the other equation is 3rd order. Thus, totally seven boundary conditions are needed to solve the governing equations. These seven boundary conditions are given by Vinson and Sierakowski [23] as

$$\begin{aligned} &v(0) = 0, \quad v(L) = 0, \quad v(0) = 0, \\ &N_x(0) = p, \quad N_x(L) = p, \quad M_x(0) = 0, \quad M_x(L) = 0 \end{aligned} \tag{28}$$

The first three are the geometric boundary conditions and the last four are the natural boundary conditions. The beam is pinned-pinned with a roller at $x = L$. Here N_x stands for the axial load and M_x for the moment. As mentioned before, the boundary conditions can be derived during the derivation of governing equations. For the different kinematic assumptions, the expressions for N_x and M_x are different. The boundary conditions due to the different kinematic assumptions differentiate only in the natural boundary conditions. N_x and M_x are expressed as

$$N_x = Au_x + Bv_{xx} - N_{xt}, \quad M_x = Bu_x + Du_{xx} - M_{xt}. \tag{29}$$

where N_{xt} is the thermo-elastic axial force and M_{xt} is the moment due to both asymmetry and thermo-elastic stress. N_{xt} and M_{xt} have the following expressions:

$$\begin{aligned} N_{xt} &= (A - E_s b_1 R_1)\alpha_c \Delta T + E_s b_1 R_1 \alpha_s \Delta T \\ M_{xt} &= \left(B - \frac{1}{2} E_s b_1 R_2\right)\alpha_c \Delta T + \frac{1}{2} E_s b_1 R_2 \alpha_s \Delta T \end{aligned} \tag{30}$$

The analytical solutions of Eqs. (18) and (19) are polynomials

$$v_{a1} = c_4 x^3 + c_5 x^2 + c_6 x, \tag{31}$$

and

$$u_{a1} = c_1 x^2 + c_2 x. \tag{32}$$

c_is can be solved by using the boundary conditions as follows:

$$\begin{aligned} c_1 &= \frac{B(M_{xt} - Bc_2 - 2Dc_5) - D(N_{xt} + p - Ac_2 - 2Bc_5)}{2L(B^2 - DA)}, \\ c_2 &= \frac{BM_{xt} - D(N_{xt} + p)}{(B^2 - DA)}, \\ c_4 &= \frac{B(N_{xt} + p - Ac_2 - 2Bc_5) - A(M_{xt} - Bc_2 - 2Dc_5)}{6L(B^2 - DA)}, \\ c_5 &= \frac{B(N_{xt} + p) - AM_{xt}}{2(B^2 - DA)}, \\ c_6 &= -c_4 L^2 - c_5 L. \end{aligned}$$

where c_2 and c_5 are the two independent coefficients. All other coefficients are expressed by them. The reason to give the solutions of Eqs. (18) and (19) is that they are the solutions of Eqs. (26) and (27) when there is no axial load. The detailed solution procedure on how to obtain the solution of the linear equation set is given in Appendix. The analytical solutions of Eqs. (26) and (27) depend on the parameter γ and γ is defined as $\gamma = \frac{-\alpha}{1 - \frac{\beta^2}{\alpha_1}}$. If $\gamma = 0$, it indicates no axial load. When there is no axial load, the solutions of Eqs. (26) and (27) have the same form of Eqs. (31) and (32).

When $\gamma > 0$ (also $\alpha < 0$), which indicates that the beam is under compression, the solutions of Eqs. (26) and (27) are

$$V_{a2} = d_1 + d_2\zeta + d_3 \sin(k\zeta) + d_4 \cos(k\zeta), \tag{33}$$

and

$$U_{a2} = \frac{\beta k}{\alpha_1}[d_3 \cos(k\zeta) - d_4 \sin(k\zeta)]d_5\zeta^2 + d_6\zeta + d_7. \tag{34}$$

Here k is defined as $k = \sqrt{\gamma}$. d_is ($i = 1$–7) are the constants solved by using the boundary conditions as follows:

$$d_4 = \frac{B(N_{xt}+p) - AM_{xt}}{A\left(\frac{B\beta k^2}{\alpha_1}+\frac{Dk^2}{L}\right) - B\left(\frac{A\beta k^2}{\alpha_1}+\frac{Bk^2}{L}\right)},$$

$$d_6 = \frac{\left(\frac{B\beta}{\alpha_1}+\frac{D}{L}\right)K^2(N_{xt}+p) - \left(\frac{A\beta}{\alpha_1}+\frac{B}{L}\right)k^2M_{xt}}{A\left(\frac{B\beta k^2}{\alpha_1}+\frac{Dk^2}{L}\right) - B\left(\frac{A\beta k^2}{\alpha_1}+\frac{Bk^2}{L}\right)},$$

$$d_3 = \frac{Bk_3 - Ak_5}{k^2\sin(k)\left[A\left(\frac{B\beta}{\alpha_1}+\frac{D}{L}\right) - B\left(\frac{A\beta}{\alpha_1}+\frac{B}{L}\right)\right]},$$

$$d_5 = \frac{k_3\left(\frac{B\beta}{\alpha_1}+D\right) - k_5\left(\frac{A\beta}{\alpha_1}+B\right)}{2\left[A\left(\frac{B\beta}{\alpha_1}+\frac{D}{L}\right) - B\left(\frac{A\beta}{\alpha_1}+\frac{B}{L}\right)\right]},$$

$$d_1 = -d_4, \quad d_2 = -d_1 - d_3\sin(k) - d_4\cos(k), \quad d_7 = -\frac{\beta k}{\alpha_1}d_3,$$

with k_3 and k_5 defined as

$$k_3 = N_{xt} + p + \left(\frac{A\beta}{\alpha_1}+\frac{B}{L}\right)k^2\cos(k)d_4 - Ad_6,$$

$$k_5 = M_{xt} + \left(\frac{B\beta}{\alpha_1}+\frac{D}{L}\right)k^2\cos(k)d_4 - Bd_6.$$

If $\gamma < 0$ (also $\alpha > 0$), which indicates the beam under tension, the solutions are now changed as

$$V_{a2} = f_1 + f_2\zeta + f_3\sinh(k\zeta) + f_4\cosh(k\zeta), \tag{35}$$

and

$$U_{a2} = \frac{\beta k}{\alpha_1}[f_3\cosh(k\zeta) + f_4\sinh(k\zeta)] + f_5\zeta^2 + f_6\zeta + f_7. \tag{36}$$

Now k is redefined as $k = \sqrt{-\gamma}$. Constants f_is ($i = 1$–7) are also solved by using the boundary conditions as follows

$$f_4 = d_4, \quad f_6 = d_6, \quad f_3 = \frac{Bk_3' - Ak_5'}{k^2\sinh(k)\left[-A\left(\frac{B\beta}{\alpha_1}+\frac{D}{L}\right) + B\left(\frac{A\beta}{\alpha_1}+\frac{B}{L}\right)\right]},$$

$$f_5 = \frac{k_3'\left(\frac{B\beta}{\alpha_1}+\frac{D}{L}\right) - k_5'\left(\frac{A\beta}{\alpha_1}\frac{B}{L}\right)}{2\left[-A\left(\frac{B\beta}{\alpha_1}+\frac{D}{L}\right) + B\left(\frac{A\beta}{\alpha_1}+\frac{B}{L}\right)\right]},$$

$$f_1 = -f_4, \quad f_2 = -f_1 - f_3\sinh(k) - f_4\cosh(k), \quad f_7 = -\frac{\beta k}{\alpha_1}f_3,$$

with k_3' and k_5' defined as

$$k_3' = N_{xt} + p - \left(\frac{A\beta}{\alpha_1}+\frac{B}{L}\right)k^2\cosh(k)f_4 - Af_6,$$

$$k_5' = M_{xt} - \left(\frac{B\beta}{\alpha_1}+\frac{D}{L}\right)k^2\cosh(k)f_4 - Bf_6.$$

To compare the solutions of the linear equations (v_{a1} and u_{a1}) derived from kinematic assumption 1 and those of the linear parts of the equations derived from kinematic assumption 2 or 3 (V_{a1} and U_{a2}), the beam length L is taken as 1 m for the statement convenience. Thus, the dimensional and dimensionless deflections derived from the same equations have the same values. Here the other related parameters are taken as

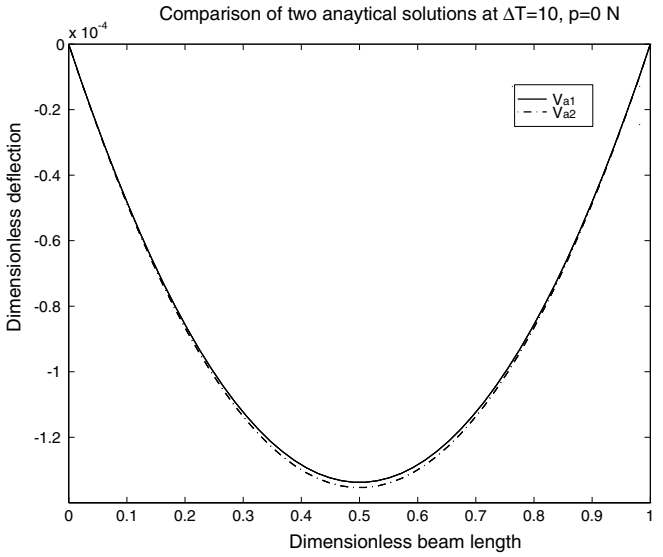

Fig. 3. The deflection comparison of two different analytical solutions of linear equations derived from two different kinematic assumptions at $\Delta T = 10\ ^\circ\mathrm{C}$ and no mechanical loading of $p = 0$ N.

$$E_c = 3.78\times10^{10}\ \mathrm{Pa}, \quad E_s = 78.5\times10^{10}\ \mathrm{Pa},$$
$$\alpha_c = 0.4\times10^{-6}\ ^\circ\mathrm{C}^{-1}, \quad \alpha_s = 6.61\times10^{-6}\ ^\circ\mathrm{C}^{-1}.$$
$$b = 0.01\ \mathrm{m}, \quad h_1 = 0.02\ \mathrm{m}, \quad h_2 = 0.0\ \mathrm{m},$$
$$h_3 = 0.02\ \mathrm{m}, \quad h_4 = 0.02\ \mathrm{m}.$$

In this paper, we directly change the parameters h_is ($i = 1$–4) to study the composite beam, which are determined by the beam dimensions (b, b_1, b_2 and H_is). And the relationship between H_i and h_i is shown in Figs. 1 and 2. The normal procedure is to give the beam dimensions first and then compute h_is. But this will not be convenient for our study. Because b_1 and b_2 are also the parameters to determine h_1 in Eq. (1) and $b = b_1 + 2b_2$, once b and h_is (or H_is) are given, b_1 (or b_2) can be computed from Eq. (1), correspondingly.

As shown in Figs. 3 and 4, the solutions of v_{a1} are always smaller than those of V_{a2} (because $L = 1$ m, dimensional v_{a1} and dimensionless V_{a1} have the same value). The reason is that in the governing equations for v_{a1}, the axial compression, which reduces the bending stiffness of the beam, is not incorporated. In Fig. 3, $p = 0$ N and $\Delta T = 10\ ^\circ\mathrm{C}$, in which only a small amount of thermal compression is exerted. In Fig. 4, relatively much larger compression is exerted. The mechanical compression force is $p = -2000$ N, which is about 8% of the buckling load and $\Delta T = 30\ ^\circ\mathrm{C}$ the two analytical solutions of the linear equations, v_{a1} and V_{a2}, have already shown very significant difference.

3.2. Numerical methods and results of the nonlinear equations

To solve the nonlinear Eqs. (24) and (25), U and V are assumed to have the following expansions:

$$U = \sum_{i=1}^{n} a_i\sin(i\pi\zeta) + U_{a2}, \tag{37}$$

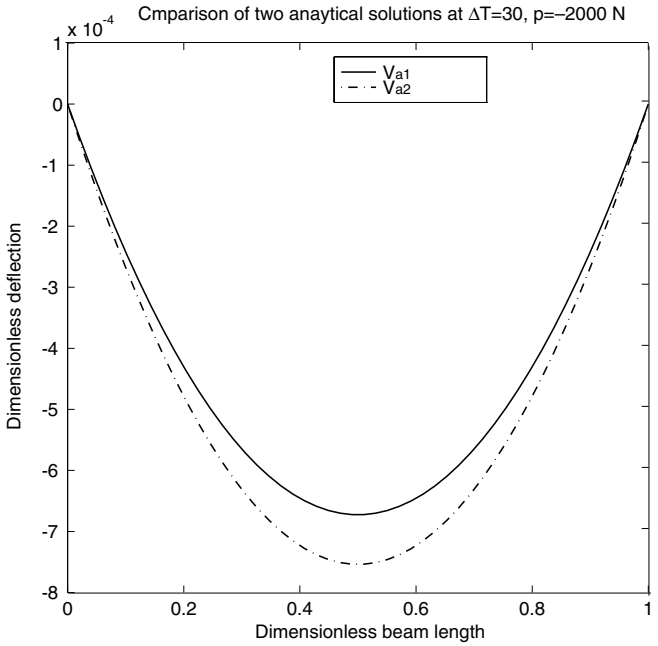

Fig. 4. The deflection comparison of two different analytical solutions of linear equations derived from two different kinematic assumptions at $\Delta T = 10\ ^\circ\mathrm{C}$ and the compressive mechanical load $p = -2000$ N.

and

$$V = \sum_{i=1}^{n} b_i \sin(\mathrm{i}\pi\zeta) + V_{\mathrm{a}2}. \tag{38}$$

Here n is mode number, $U_{\mathrm{a}2}$ and $V_{\mathrm{a}2}$ have two roles. First, they are the solutions of the beam axial displacement and the transverse displacement of the linear theory. The other sine terms in the Galerkin series behave mathematically like the perturbation terms to rectify $U_{\mathrm{a}2}$ and $V_{\mathrm{a}2}$ for the nonlinear governing equations. Second, their very existence makes V and U to satisfy boundary conditions. Now if sin(iπζ) times Eqs. (24) and (25) and integrates from 0 to 1, the following equation is obtained after some simple manipulations:

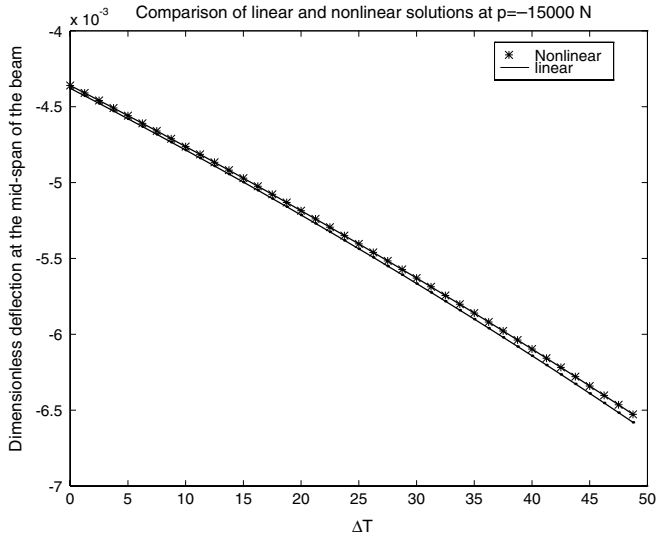

Fig. 5. The deflection comparison of linear and nonlinear solutions when $p = -15{,}000$ N as ΔT changes.

If plugging U and V expansions of Eqs. (37) and (38) into Eq. (39), the previous nonlinear differential equations are now transformed into the set of polynomials of a_i, and b_i. It is a set of $2n$ equations for $2n$ unknowns (a_i, and b_i, $i = 1, 2 \ldots n$). The solutions are obtained by using Newton–Rhapson iteration method.

The nonlinear effect depends on how large the beam deflects. One fact is also noticed that in both Eqs. (24) and (25), all nonlinear terms are governed by one coefficient η. η is the parameter related to g_0, temperature and the coefficients of thermal expansion. Increasing the compression load has two effects. The first is to reduce the structural stiffness, thus to enlarge deflection. The other is to increase parameter η, which increases the nonlinear influence on the structural deflection. Increasing compression makes the difference enlarge between nonlinear and linear solutions. In Figs. 5 and 6, we show how such difference between nonlinear and linear solutions enlarges as ΔT

$$\begin{cases}
\int_0^1 \sin(\pi\zeta)\left[\beta V_{\zeta\zeta\zeta} - \alpha_1 U_{\zeta\zeta} - \eta V_\zeta V_{\zeta\zeta} - \beta\left(V_\zeta V_{\zeta\zeta}^2 + \frac{V_\zeta^2 V_{\zeta\zeta}}{2}\right)\right] \mathrm{d}\zeta = 0 \\
\int_0^1 \sin(2\pi\zeta)\left[\beta V_{\zeta\zeta\zeta} - \alpha_1 U_{\zeta\zeta} - \eta V_\zeta V_{\zeta\zeta} - \beta\left(V_\zeta V_{\zeta\zeta}^2 + \frac{V_\zeta^2 V_{\zeta\zeta}}{2}\right)\right] \mathrm{d}\zeta = 0 \\
\vdots \\
\int_0^1 \sin(n\pi\zeta)\left[\beta V_{\zeta\zeta\zeta} - \alpha_1 U_{\zeta\zeta} - \eta V_\zeta V_{\zeta\zeta} - \beta\left(V_\zeta V_{\zeta\zeta}^2 + \frac{V_\zeta^2 V_{\zeta\zeta}}{2}\right)\right] \mathrm{d}\zeta = 0 \\
\int_0^1 \sin(\pi\zeta)\left[V_{\zeta\zeta\zeta\zeta} - \beta U_{\zeta\zeta\zeta} - \alpha V_{\zeta\zeta} - \eta\left(U_{\zeta\zeta} V_\zeta + U_\zeta V_{\zeta\zeta} + \frac{3}{2} V_\zeta^2 V_{\zeta\zeta}\right)\right] \mathrm{d}\zeta = 0 \\
\int_0^1 \sin(2\pi\zeta)\left[V_{\zeta\zeta\zeta\zeta} - \beta U_{\zeta\zeta\zeta} - \alpha V_{\zeta\zeta} - \eta\left(U_{\zeta\zeta} V_\zeta + U_\zeta V_{\zeta\zeta} + \frac{3}{2} V_\zeta^2 V_{\zeta\zeta}\right)\right] \mathrm{d}\zeta = 0 \\
\vdots \\
\int_0^1 \sin(n\pi\zeta)\left[V_{\zeta\zeta\zeta\zeta} - \beta U_{\zeta\zeta\zeta} - \alpha V_{\zeta\zeta} - \eta\left(U_{\zeta\zeta} V_\zeta + U_\zeta V_{\zeta\zeta} + \frac{3}{2} V_\zeta^2 V_{\zeta\zeta}\right)\right] \mathrm{d}\zeta = 0
\end{cases} \tag{39}$$

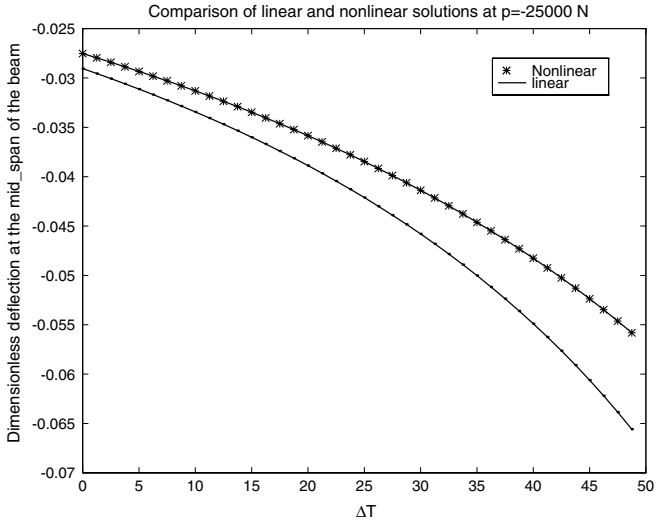

Fig. 6. The deflection comparison of linear and nonlinear solutions when $p = -25{,}000$ N as ΔT changes.

varies. The linear solution is V_{a2} (at $\xi = \frac{1}{2}$) of Eq. (33) for the compressive load case, which physically is the deflection of the midspan. In Figs. 5 and 6, p is fixed as $-15{,}000$ and $-25{,}000$ N, respectively.

3.3. The influences of the shift of SMA layer from the neutral axis and SMA layer thickness on the deflection

If the SMA thickness is fixed, the SMA layer shift from the neutral axis will increase the moment (both mechanical and thermo-mechanical) exerted on the beam if the loadings are keep unchanged. This makes the beam to bend more. Keep the SMA layer thickness H_2 fixed at 0.02 m. The following three cases are compared. Case 1: $h_2 = -0.01$ m (SMA layer is in the center of the beam, the symmetric beam). Case 2: $h_2 = -0.005$ m, case 3: $h_2 = 0$ m. Cases 2 and 3 are the asymmetric beams. When the SMA layer is in the center, the mechanical and thermo-mechanical stresses are symmetrically distributed on the cross-section; thus no moment is generated. As a result, the beam remains straight. More the SMA layer is shifted away from the neutral axis, more the moment due to asymmetry is generated. Then the beam bends more. In Fig. 7, this effect is well reflected. Mechanical load p and thermo-mechanical load both enlarge the deflections of the three cases.

If $H_3 = 0.02$ m is fixed change the thickness of the SMA layer (H_2) from 0.005 m to 0.01 m to 0.02 m. The increment of the thickness has two effects on the deflection. Because Young's moduli of SMA and epoxy are different (here $E_s > E_c$), the first effect of increasing the SMA thickness is to increase the whole beam bending stiffness. At the same time, it also makes the parameter B bigger. So the second effect is that at the same temperature, more moment is generated. These two effects compete to determine whether the beam bends more or less. For this competition, the difference between epoxy and SMA Young's moduli is vital. For the first scenario we study here, Young's moduli for epoxy and SMA are taken as $E_c = 3.78 \times 10^{10}$ Pa, $E_s = 78.5 \times 10^{10}$ Pa, in which there is a very large difference between Young's Moduli of the two materials. The result is that the case with $H_2 = 0.02$ m bends less than the case with $H_2 = 0.01$ m

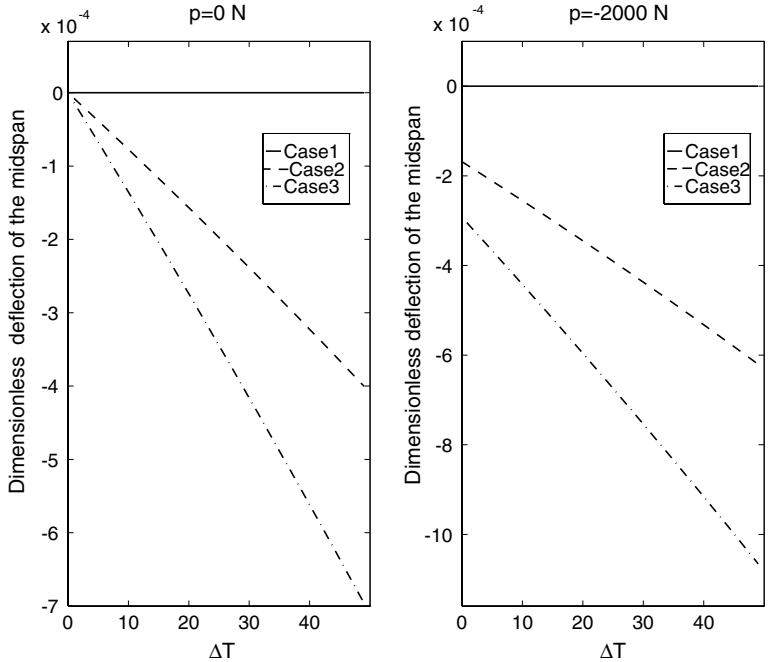

Fig. 7. The study of asymmetry influence on the beam deflection. The three cases have the different deviations from the neutral axis. Case 1 is the symmetric one, which has no deviation.

though it has larger bending moment, but its bigger bending stiffness counteracts for that. In a word, the increment of the bending moment is less than the increment of the bending stiffness as the SMA layer thickness increases. The results are shown in Fig. 8 and hold for both $p = 0$ N and $p = -2000$ N cases as ΔT increases from 0 to 50 °C. For this scenario of the very large difference in Young's moduli of the two materials, increasing the thickness will not necessarily increase the deflection.

If Young's moduli for epoxy and SMA are $E_c = 53.78 \times 10^{10}$ Pa, $E_s = 78.5 \times 10^{10}$ Pa, then the two materials Young's moduli are close to each other. For this scenario, the results are shown in Fig. 9 for both $p = 0$ N and $p = -2000$ N cases with ΔT increasing. For this scenario of the materials with much less difference in Young's modulus, the bending moment increases faster than the bending stiffness when the SMA layer thickness increases. Increasing SMA layer thickness means more deflection for this scenario.

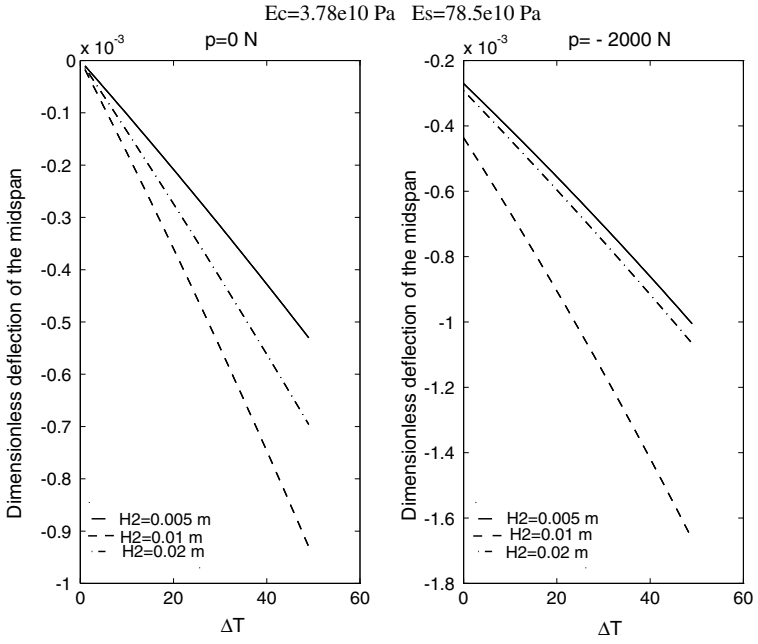

Fig. 8. The study of SMA thickness influence on the beam deflection. For this study, there is relatively large difference in Young's moduli of SMA and epoxy.

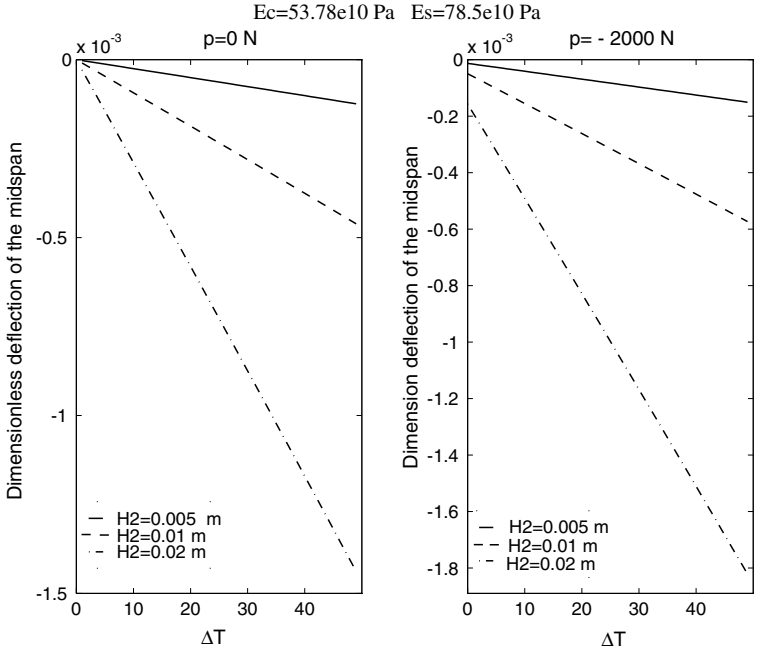

Fig. 9. The study of SMA thickness influence on the beam deflection. For this study, there is relatively a small difference in Young's moduli of SMA and epoxy.

The best way to analyze the influence of the competition between bending moment and stiffness on the deflection for the different SMA layer thicknesses is to analyze the derivatives of V_{a2}. As V_{a2} is the function with the multi-variables, the derivatives of V_{a2} with respect to thickness, temperature and h_2 are numerically computed and are shown in Fig. 10, respectively. h_2 is the parameter indicating the distance between the SMA layer lower edge and the neutral axis. In Fig. 10, $E_c = 3.78 \times 10^{10}$ Pa, $E_s = 78.5 \times 10^{10}$ Pa, $p = 0$ N and $H_3 = 0.02$ m. The first plot in Fig. 10 shows that $\frac{\partial V_{a2}}{\partial H_2}$, the deflection derivative with respect to the SMA layer thickness (H_2) goes from the negative to the positive numbers. Because the deflection of the beam is a negative value, the positive derivative is to reduce the magnitude of deflection. This positive derivative value scenario is also reflected in Fig. 8. For both $\frac{\partial V_{a2}}{\partial \Delta T}$ and $\frac{\partial V_{a2}}{\partial h_2}$ shown in the 2nd and 3rd plots of Fig. 10, the derivatives are always negative, which means increasing either ΔT or h_2 can only increase the beam deflection magnitude.

4. Buckling, post-buckling analysis and finite element method

4.1. A brief discussion on the usage of Galerkin method in buckling and post-buckling analysis of a composite beam

Compared with Rayleigh–Ritz method, Galerkin method (also called method of weighting functions) is to minimize the sequence consisting of admissible functions rather than comparison functions [25,26]. In Galerkin method, the boundary conditions information is included in the expansion series. The expansion series usually are the mode shapes. Sine expansion series are actually the mode shapes derived from the linear vibration equation of the homogeneous pinned-pinned beam, which is a self-adjoint system. As the expansion forms shown in Eqs. (37) and (38), the sine function, which is derived from the governing equation of a self-adjoint system, is guaranteed to the admissible function. Eqs. (37) and (38) are

$$U = \sum_{i=1}^{n} a_i \sin(i\pi\zeta) + U_{a2}, \tag{37}$$

and

$$V = \sum_{i=1}^{n} b_i \sin(i\pi\zeta) + V_{a2}. \tag{38}$$

For both Rayleigh–Ritz method and Galerkin method, the expansion functions of comparison function or admissible function are needed to satisfy the boundary conditions. Without U_{a2} and V_{a2} in U and V expansions, the sine terms in U and V will lead to the boundary conditions that the moments at the ends are zero, which is only true for the symmetric beam case. With U_{a2} and V_{a2} in Eqs. (37) and (38), the boundary conditions of both the symmetric and the asymmetric cases can be

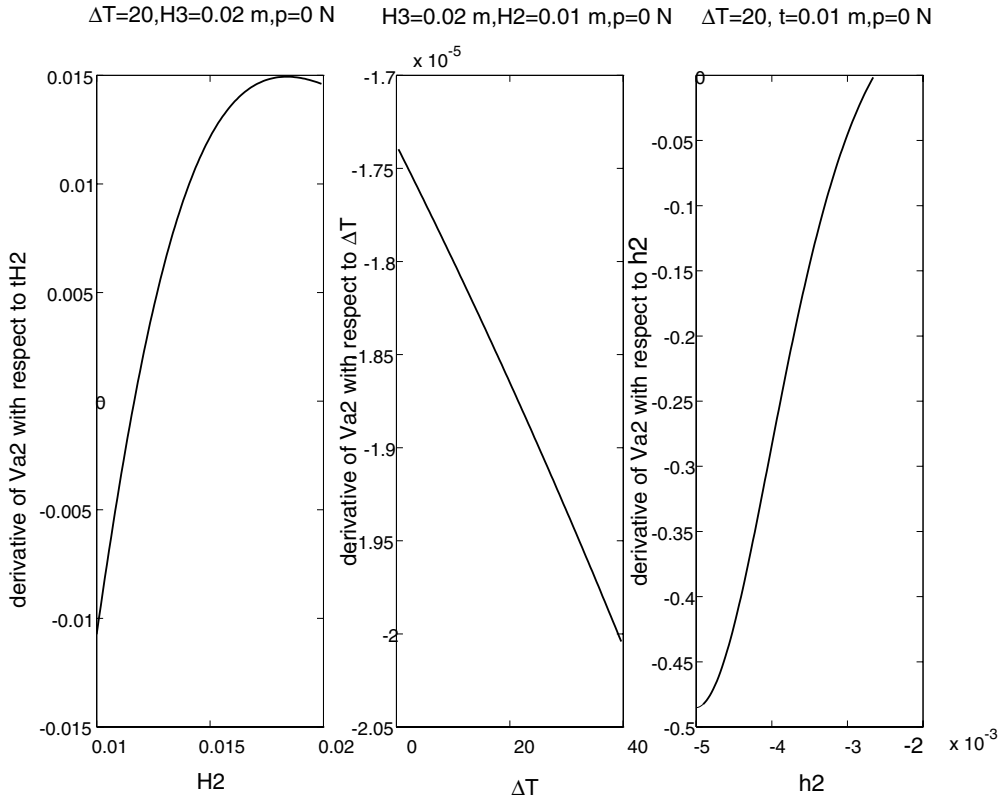

Fig. 10. The derivatives of V_{a2} with respect to H_2, ΔT and h_2, respectively. The parameters in this figure are the same as those in Fig. 8.

satisfied, which is discussed before. While U_{a2} and V_{a2} are the solutions of the linear equations, which become singular at buckling. The singularity of U_{a2} and V_{a2} prevents us from using Galerkin method for the post-buckling analysis. In the text that follows, a discussion is made on the singularity.

Eqs. (24) and (25) are well suitable for the buckling and post-buckling analysis. While if the equations above are discretized by Galerkin method as Eq. (39), then there is some numerical difficulty in the post-buckling analysis. Let us analyze the solution form to find out why. For the buckling and post-buckling analysis, the axial force in both Eqs. (24) and (25) is compressive, i.e., $\gamma < 0$. So for the transverse displacement V, the solution of Eq. (33) is the solution form for V_{a2} and Eq. (33) is

$$V_{a2} = d_1 + d_2\zeta + d_3\sin(k\zeta) + d_4\cos(k\zeta). \tag{33}$$

The constant d_3 is defined before as

$$d_3 = \frac{Bk_3 - Ak_5}{k^2\sin(k)\left[A\left(\frac{B\beta}{\alpha_1}+\frac{D}{L}\right) - B\left(\frac{A\beta}{\alpha_1}+\frac{B}{L}\right)\right]}$$

$k = \sqrt{\gamma}$. So if $\gamma = n^2\pi^2$ (n is an integer), then d_3 is singular. For symmetric beam of $B = 0$, we can directly use the above equation to find the buckling load. For symmetric beam

$$\gamma = -\alpha = n^2\pi^2$$

where α as defined before is directly related with the axial loads. This is the exact solution of the buckling load values (here they are dimensionless) derived from the classical buckling analysis for the pinned-pinned beam under compression [27,28]. π^2 is the lowest buckling load value. The reason that the axial displacement U does not affect the buckling load at all for the symmetric beam is that when $B = 0$ (also $\beta = 0$), Eqs. (26) and (27) are uncoupled. When $\beta = 0$, Eq. (27) is the governing equation for the classical buckling analysis [27,28]. For the asymmetric beam ($\beta \neq 0$), the singularity condition is

$$\gamma = \frac{-\alpha}{1 - \frac{\beta^2}{\alpha_1}} = n^2\pi^2$$

The asymmetry here actually plays the same role as the geometric imperfection plays in the classical buckling analysis though there is some difference in their governing equations. For straight/symmetric beam, or say, the beam without imperfection, the beam remains straight (no deflection) before and upon the buckling during the compressive loading. For the asymmetric beam or say the beam with imperfection (unstraight beam), the beam deflects instantly once there is axial loading.

So it is clear now that as the compressive load reaches the buckling value, V_{a2} becomes singular. This singularity property can be used for buckling analysis to predict buckling load. V_{a2} is a solution of linear equations and the linear analysis results in the singularity at buckling. Physically, as exhibited by the nonlinear analysis, the buckling beam continuously deflects in post-buckling region with the finite magnitude. So the Galerkin method used here cannot be applied to post-buckling region due to the singularity of V_{a2}. For the compressive load less than the buckling load, Galerkin method used here performs well and Galerkin method should be restricted in pre-buckling region.

The way out is to seek other discretization methods. As the analysis shown in Section 2, our approach actually is to model the composite beam as "stressfully equivalent" [17,18] homogeneous beam and the numerical difficulty is due to the singularity of one expansion term in Galerkin method. The mode shape of the composite beam can be very different from that of the homogeneous beam due to coupling. Banerjee shows an example of how complex and different the mode shapes of a composite beam can be compared with those of a homogeneous beam [29]. Those mode shapes of the composite beam may avoid the singularity of the expansion terms in Galerkin method. For such composite beam mode shape analysis, it is beyond the scope of this paper. In this paper, finite element (FE) method is adopted to avoid such singularity problem in numerical computation.

4.2. Finite element analysis for the composite beam post-buckling analysis

Galerkin method used here needs V_{a2} as an expansion term and it blows up at buckling load. As a discretization method, FE method can avoid such numerical problem. In Galerkin method, the boundary condition information is included in the expansion functions. While for FE method, it is to deal with the nodes at the ends to enforce the boundary conditions. And for the linear FE analysis, the boundary condition can be directly enforced during the (stiffness, mass, damping, etc.) matrices assembling. The interpolation function of FE method is polynomial. The singularity due to enforcing the boundary conditions in Galerkin method does not exist in FE method. For FE method, the potential energies in SMA layer and epoxy remain the same as those of

$$U_s = \frac{1}{2}\int_0^L \int_{A_M} E_s(\epsilon - \alpha_s\Delta T) + \sigma_p]\epsilon\, dA_M\, dx, \tag{16}$$

and

$$U_c = \frac{1}{2}\int_0^L \int_{A_c} E_c(\epsilon - \alpha_c\Delta T)]\epsilon\, dA_c\, dx. \tag{17}$$

By applying the principle of minimum potential energy (PMPE, $\delta U = \delta U_c + \delta U_s = 0$) and plugging the ϵ of kinematic assumption 2, the following integral equation is obtained:

$$\delta U = \delta U_c + \delta U_s = \frac{E_c}{2}\int_0^L \int_{A_c} \left\{ 2g_0\delta u_x + 2u_x\delta u_x + 2g_0 v_x\delta v_x + v_x^2\delta u_x + 2u_x v_x\delta v_x + v_x^3\delta v_x - 2y\left(g_0 + u_x + \frac{v_x^2}{2}\right)\delta v_{xx} \right.$$
$$-2yv_{xx}(\delta u_x + v_x\delta v_x) + 2y^2 v_{xx}\delta v_{xx} - \alpha_c\Delta T(\delta u_x + v_x\delta v_x - y\delta v_{xx})\big\}\,\mathrm{d}A_c\,\mathrm{d}x + \frac{E_s}{2}\int_0^L \int_{A_s} \{2g_0\delta u_x + 2u_x\delta u_x + 2g_0 v_x\delta v_x$$
$$+v_x^2\delta u_x + 2u_x v_x\delta v_x + v_x^3\delta v_x - 2y\left(g_0 + u_x + \frac{v_x^2}{2}\right)\delta v_{xx} - 2yv_{xx}(\delta u_x + v_x\delta v_x) + 2y^2 v_{xx}\delta v_{xx} - \alpha_c\Delta T(\delta u_x + v_x\delta v_x - y\delta v_{xx})\Big\}$$
$$\mathrm{d}A_M\,\mathrm{d}x - \frac{E_s}{2}\int_0^L \int_{A_M} \alpha_s\Delta T(\delta u_x + v_x\delta v_x - y\delta v_{xx})\,\mathrm{d}A_M\,\mathrm{d}_x + \frac{1}{2}\int_0^L \int_{A_M} \sigma_p(\delta u_x + v_x\delta v_x - y\delta v_{xx})\,\mathrm{d}A_M\,\mathrm{d}x = 0 \tag{40}$$

Unlike Galerkin method, which operates two more integrations by parts procedures after the variational operation, the integral Eq. (40) for FE analysis is obtained only after one variational operation. For FE method, the following polynomial interpolation functions are introduced [30]:

$$B_1 = 1 - \xi, \quad B_2 = \xi,$$
$$N_1 = 1 - 3\xi^2 + 2\xi^3, \quad N_2 = L_e\xi(1 - 2\xi + \xi^2),$$

and

$$N_3 = \xi^2(3 - 2\xi), \quad N_4 = L_e\xi^2(\xi - 1).$$

with $\xi = \frac{x}{L_e}$, L_e is the element length. Now the axial and transverse displacements $\vec{H}^T = (u, v)$ (superscript T for transpose) in one element are approximated as

$$\vec{H} = \begin{pmatrix} u \\ v \end{pmatrix} = \begin{pmatrix} B_1 & 0 & 0 & B_2 & 0 & 0 \\ 0 & N_1 & N_2 & 0 & N_3 & N_4 \end{pmatrix} \begin{pmatrix} u_1 \\ v_1 \\ \theta_1 \\ u_2 \\ v_2 \\ \theta_2 \end{pmatrix} \tag{41}$$

u_i, v_i, θ_i ($i = 1, 2$) are the nodal axial displacement, transverse displacement and rotation angle of the element, respectively. Plug these interpolation functions forms of u and v into Eq. (40), the FE equation of u_i, v_i, θ_i is derived. For n elements (thus $n + 1$ nodes), there are $3 \times (n + 1)$ equations for $3 \times (n + 1)$ unknowns of u_i, v_i, θ_i ($i = 1$, $n + 1$); Newton–Rhapson method is also used here to solve Eq. (40). If linear analysis that only constant and linear terms are kept in Eq. (40), then LU decomposition method is applied for this linear algebra problem solution.

4.3. Results and discussion of buckling and post-buckling analysis

Here as the recovery stress is incorporated, we assume that the ambient temperature is 0 °C and thus $T = \Delta T$ for the statement convenience. In Fig. 11, a comparison of FE linear and nonlinear solutions with the analytical solution is made as T changes. The beam is asymmetric with the parameters $L = 1$ m, $h1 = 0.00149$ m, $h2 = 0.00151$ m, $h3 = 0.002$ m, $h4 = 0.002$ m. In Fig. 11, it is shown that both FE linear solution and analytical solution blow up around the buckling temperature of the symmetric beam (in Fig. 11, only the part of linear solution with the small magnitude is shown). It is noticed that after buckling, both FE linear solution and analytical solution change signs, while the nonlinear solution changes continuously. The sign change around the buckling point misses one solution of the composite beam as the linear analysis can no longer be valid after buckling. That is also another reason why the Galerkin expansion form cannot be applied in post-buckling analysis. For all the analyses in this buckling and post-buckling analysis section, $E_s = 20.5 \times 10^{10}$ Pa and $E_c = 53.78 \times 10^{10}$ Pa.

For comparison purpose, the fourth order differential equation of classical buckling analysis is given as follows [28]:

$$\mathrm{EI}y_{xxxx} - P_e y_{xx} = 0 \tag{42}$$

where EI is the effective bending stiffness of the composite beam, here it is D, P_e is the effective axial load, including the mechanical, thermo-mechanical forces and the force

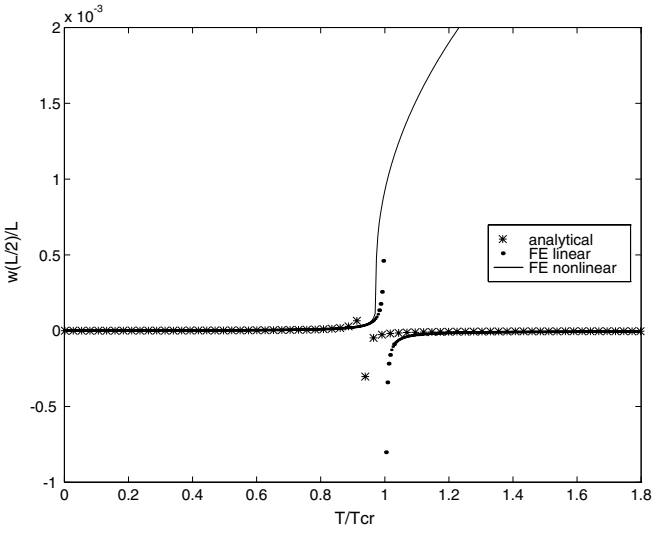

Fig. 11. The comparison of FE linear, nonlinear solutions and analytical solutions of the asymmetric beam. The beam parameters here are $L = 1$ m, $h_1 = 0.00149$ m, $h_2 = 0.00151$ m, $h_3 = 0.002$ m, $h_4 = 0.002$ m.

due to SMA phase transformation, $P_e > 0$ is tensile and $P_e < 0$ is compressive. Eq. (42) can be rewritten as

$$Dv_{xxxx} - \left(P - \frac{\Delta T}{2}(E_s\alpha_s A_M + E_c\alpha_c A_c) + \frac{\sigma_p A_M}{2}\right)v_{xx} = 0 \quad (43)$$

The recovery stress σ_p (Pa) is taken from the experimental data of Cross et al. [7] and approximated as the following

$$\sigma_p = \begin{cases} 3.5\times10^6(T-32.5) & 32.5\,^\circ\mathrm{C} \leqslant T < 42.5\,^\circ\mathrm{C} \\ 6.57\times10^6(T-42.5)+3.5\times10^7 & 42.5\,^\circ\mathrm{C} \leqslant T < 73.5\,^\circ\mathrm{C} \\ 0.884\times10^6(T-73.5)+2.3867\times10^8 & T \geqslant 73.5\,^\circ\mathrm{C} \end{cases} \quad (44)$$

For different initial conditions and processing (heating or cooling down), the recovery stress can be different. Clearly the recovery stress given above has three stages (different slopes) for the experimental data of the recovery stress given by Cross et al. [7]. The multi-stage phenomenon is one of the characteristics of SMA recovery stress. It is a common phenomenon for the composite beam with the SMA layer to get buckled, unbuckled and rebuckled during heating process [9]. This multi-stage change of the recovery stress and its competition with the (compressive) thermal load are responsible for this phenomenon. For the straight symmetric pinned-pinned beam (beam without imperfection), the lowest buckling load is [28]

$$P_b = -\frac{\pi^2 D}{L}. \quad (45)$$

By plugging in the expression of P_e and $P_e = P_b$ at buckling, we obtain

$$P_e = p - \frac{\Delta T}{2}(E_s\alpha_s A_M + E_c\alpha_c A_c) + \frac{\sigma_p A_M}{2} = P_b. \quad (46)$$

which indicates the interaction and relation of the mechanical, thermo-elastic forces and the force due to phase transformation at buckling. Before we show the buckling, unbuckling and re-buckling phenomenon as the temperature changes and the SMA layer recovery stress is activated, we show the competition between the tensile recovery stress and compressive thermal stress of Eq. (46) in Fig. 12. In Fig. 12, the beam has the following dimensions: $L = 0.457$ m, $b = b1 = 0.025$ m, $h1 = h2 = 0.0015$ m, $h3 = h4 = 0.002$ m and it is a straight symmetric beam. T_{cr} is the buckling temperature of the beam with no SMA layer embedded and no mechanical loading exerted case. P_{cr} is the mechanical buckling of the beam with no SMA layer embedded and $T = 0\,^\circ$C case. The beam with no SMA layer has the dimensions of $L = 0.457$ m, $b = 0.025$ m and the thickness of 0.004 m. And $T_{cr} = 23.1\,^\circ$C and $P_{cr} = -3388.65$ N. P is the additional mechanical load needed for the buckling. For the beam with no SMA layer, it is a straight line with the slope of -1. For the composite beam with the SMA layer embedded, the curve is quite different because the SMA layer is activated. As the nonlinear FE analysis shown in Fig. 13, the beam

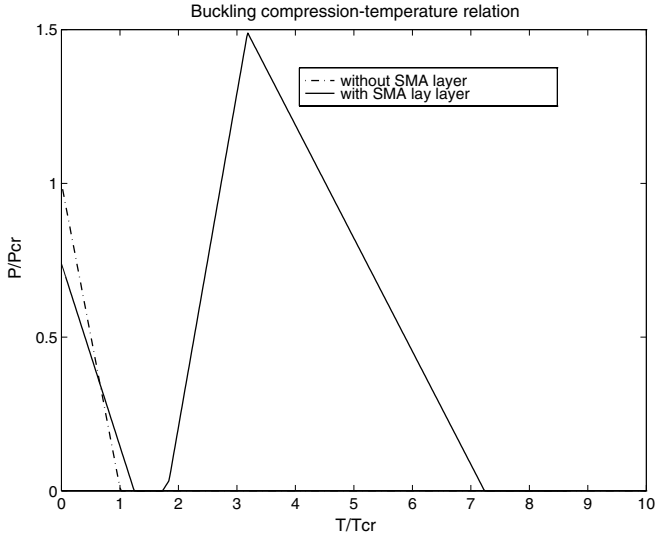

Fig. 12. The relation of the buckling compression and temperature of the symmetric composite beams with and without the SMA layer. The beam parameters here are: $L = 0.457$ m, $h_1 = h_2 = 0.0015$ m, $h_3 = h_4 = 0.002$ m. SMA is activated at $T = 32.5\,^\circ$C.

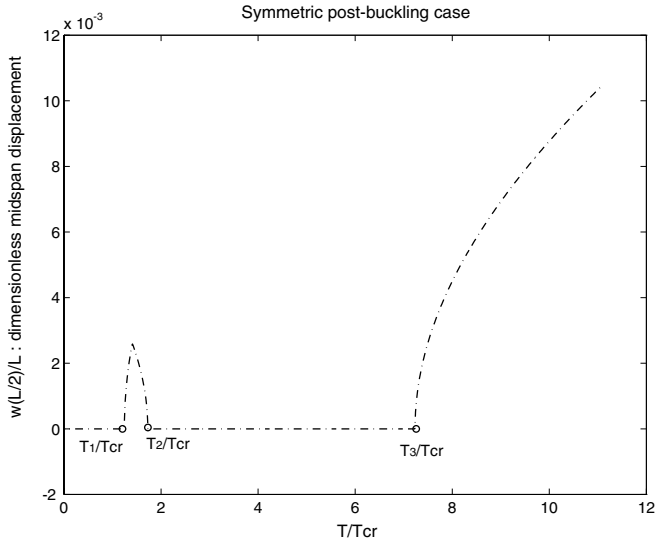

Fig. 13. The post-buckling behavior of the symmetric composite beam with the SMA layer. The beam parameters here are the same as those in Fig. 12. Here $T_{cr} = 23.1\,^\circ$C is the buckling temperature when $p = 0$ N, $P_{cr} = -3388.65$ N is the buckling compression load when $T = 0\,^\circ$C of the same size beam with no SMA layer.

with the SMA layer experiences buckling (post-buckling), unbuckling, and buckling (post-buckling) again. In Fig. 13, all the beam dimensions are shown which are the same as those shown in Fig. 12 and the thermo- mechanical load p is 0 N. From Eq. (46), three analytical "buckling" temperatures when $p = 0$ N can be easily calculated as $T_1 = 28.78\,^\circ$C, $T_2 = 39.66\,^\circ$C, $T_3 = 167.34\,^\circ$C, which are exactly matched by our FE results. Here T_1 and T_3 are the actual buckling temperatures and T_2 is the unbuckling temperature when the beam is heating up. If cooling down,

T_1 and T_3 are the unbuckling temperatures and T_2 is the buckling temperature. The first buckling is an ordinary buckling, it is purely due to the thermo-mechanical compressive force. In Fig. 13, it is shown that after SMA is activated at $T = 32.5$ °C, the post-buckling curve begins to drop down (the deflection magnitude reduces) because the recovery stress is tensile. During the first two stages, the recovery stress increases faster than the thermo-mechanical compressive stress; the curve keeps dropping down and reaches zero when the total force in the beam is equal to the critical buckling compression load. The beam deflection keeps zero when the total force in the beam is less than the critical compression load. At stage 3, SMA recovery stress increases slower than the thermal–mechanical stress. The beam begins to accumulate compression again. At T_3, the force reaches the critical buckling compression load again, then it buckles. This exact behavior is also shown in Turner's paper [9].

The buckling, unbuckling and buckling again phenomenon may not take place for some composite beam configurations. Whether the phenomenon takes place is dependent on the competition between the compressive thermo-mechanical stress and the tensile SMA layer recovery stress. In Fig. 14, the beam dimensions are $L = 0.457$ m, $b = b1 = 0.025$ m, $h1 = h2 = 0.0015$ m, $h3 = h4 = 0.0022$ m. Thus compared with the previous beam with the thickness of 0.004 m, now the thickness is 0.0044 m. The dimensions of the beam with no SMA layer are $L = 0.457$ m, $b = 0.025$ m and the thickness of 0.0044 m, which buckles at $T_{cr} = 28.05$ °C when $p = 0$ N and $P_{cr} = -4510.3$ N when $T = 0$ °C. In Fig. 14, it is seen that the composite beam with the SMA layer can only buckle at $T = 148.25$ °C ($T/T_{cr} \approx 5.25$) if no additional external mechanical load is exerted on the beam. Fig. 15 shows is the beam buckling and post-buckling plots as T changes and p is fixed as 0 N. For the different configurations, the composite beam can have the dramatically different buckling and post-buckling responses when the beam is heated and the SMA is activated.

In Fig. 16, the asymmetric beam deflection as T changes is shown. Two cases are shown for comparison. In Fig. 16, the two asymmetric cases have the following parameters:

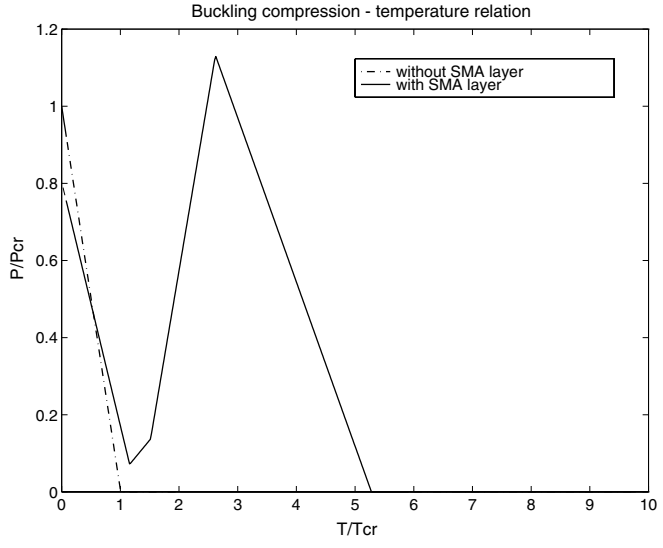

Fig. 14. The relation of buckling compression and temperature of the symmetric composite beam with and without the SMA layer. The beam parameters here are $L = 0.457$ m, $h_1 = h_2 = 0.0015$ m, $h_3 = h_4 = 0.0022$ m. $T_{cr} = 28.05$ °C is the buckling temperature of the beam with no SMA layer and no external compression of $p = 0$ N. $P_{cr} = -4510.3$ N is the buckling compression load when $T = 0$ °C of the same size beam with no SMA layer.

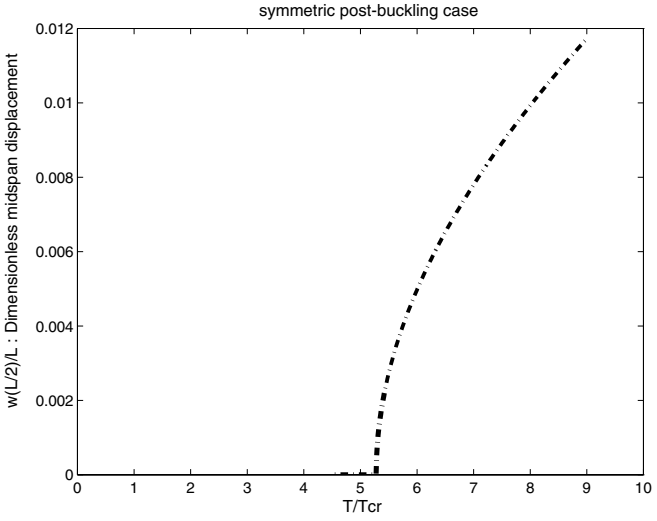

Fig. 15. The post-buckling behavior of the symmetric composite beam with the SMA layer. The beam parameters here are the same as those in Fig. 14.

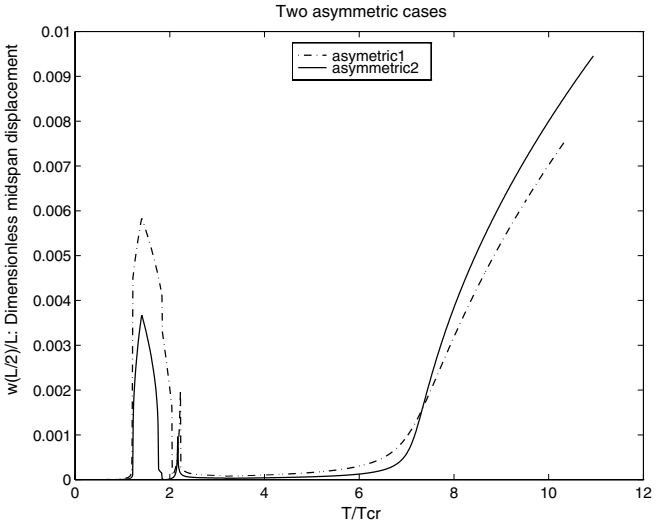

Fig. 16. The comparison of two asymmetric beam cases with the SMA layer. The beam has the same SMA and epoxy layer size as those in Fig. 14 but the different SMA layer locations.

Asymmetric case 1: $L = 0.457$ m, $h1 = 0.001496$ m, $h2 = 0.00154$ m, $h3 = h4 = 0.002$ m.
Asymmetric case 2: $L = 0.457$ m, $h1 = 0.00149$ m, $h2 = 0.00151$ m, $h3 = h4 = 0.002$ m.

Compared with the symmetric case, there is one more small peak in the asymmetric case. For the symmetric case, as far as the compression load is less than buckling load, there is no deflection. But for the asymmetric case, the moment due to eccentricity/asymmetry is always there and so is the deflection. When the beam is heated, the whole beam is under compression. In this case, since the epoxy has larger Young's modulus, the compressive force in epoxy layer is larger than that in the SMA layer. The bending moment is pointing inside (clockwise). The beam bends up. At this stage, moving the SMA layer more away from the center will have more bending moment and less stiffness for the beam. Because the SMA layer here has less Young's modulus than that of the epoxy, the configuration of having the SMA layer with smaller Young's modulus further away from the center will have smaller stiffness for the whole beam. At this stage, larger eccentricity produces larger deflection. Before SMA is activated, the increase of the bending moment and compressive thermo-mechanical force drives the beam deflection to increase. When the SMA layer is activated, the tensile recovery stress is generated. The recovery stress reduces the compression forces in both SMA and epoxy layers. As a result, the bending moment is reduced, so is the deflection. After the beam is unbuckled, the tensile recovery stress still increases faster than the compressive thermo-mechanical stress. At this stage, the whole structure is in tension. In the SMA layer, the tension is larger. With the temperature increasing, the recovery stress increases, so is the bending moment. After the deflection reaches the minimum, the deflection keeps increasing again. Soon the deflection is down again because the beam stiffness also increases due to the contribution of the tensile recovery stress. When the beam stiffness increases faster than the moment, the deflection drops down. At the same time, the recovery stress slows down and at last is surpasses by the compressive thermo-mechanical stress. At the last stage, the increase of bending moment surpassed the stiffness. The deflection begins to increase again. Also at the last stage, the deflections of the two asymmetric cases cross each other around the second buckling temperature for the symmetric beam. After the crossing, the beam with more eccentricity has less deflection. More eccentricity means more bending moment, but at this stage it also means more stiffness. Unlike the case at the beginning, though SMA has less Young's modulus, now it has the large tensile recovery stress. At this stage, the beam stiffness overcomes and surpasses the bending moment increment.

But in Fig. 17, it is seen that the beam stiffness overcomes some increment of bending moment due to eccentricity but does not surpass it. So for this scenario, more eccentricity still means more deflection. The parameters shown in Fig. 17 are

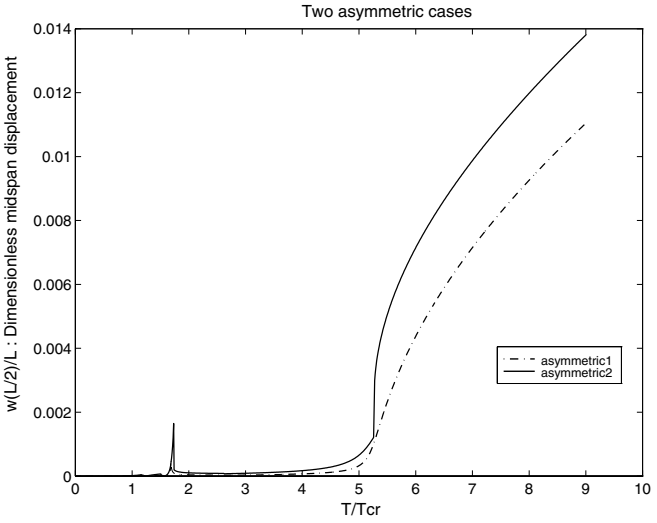

Fig. 17. The comparison of two asymmetric beam cases with the SMA layer. The beam has the same SMA and epoxy layer size as those in Fig. 15 but the different SMA layer location.

Asymmetric case 1: $L = 0.457$ m, $h1 = 0.001496$ m, $h2 = 0.00154$ m, $h3 = h4 = 0.0022$ m.
Asymmetric case 2: $L = 0.457$ m, $h1 = 0.00149$ m, $h2 = 0.00151$ m, $h3 = h4 = 0.0022$ m.

The configuration (and thus the volume fraction) of SMA shown in Figs. 16 and 17 is different. It is noticed that there are two peaks in Fig. 16 for each asymmetric case and there is only one peak in Fig. 17 for each asymmetric case.

5. Dynamic properties: free and forced vibration

5.1. Equations of motion for free vibration and natural frequency analysis

By adding the kinetic energy $K\left(K = \int_0^L \frac{m(\dot{u}^2+\dot{v}^2)}{2}\,\mathrm{d}x\right)$ and by using Hamilton's principle ($\delta(K - U_t) = 0$, U_t is the total potential energy and $U_t = U_s + U_c$), equations of motion based on kinematic assumption 3 are derived. The following is the dimensionless form of the equations of motion:

$$U_{\tau\tau} + \beta V_{\zeta\zeta\zeta} - \alpha_1 U_{\zeta\zeta} = \eta V_\zeta V_{\zeta\zeta} + \beta\left(V_\zeta V_{\zeta\zeta}^2 + \frac{V_\zeta^2 V_{\zeta\zeta}}{2}\right), \quad (47)$$

and

$$V_{\tau\tau} + V_{\zeta\zeta\zeta} - \beta U_{\zeta\zeta\zeta} - \alpha V_{\zeta\zeta} = \eta\left(U_{\zeta\zeta} V_\zeta + U_\zeta V_{\zeta\zeta} + \frac{3}{2} V_\zeta^2 V_{\zeta\zeta}\right). \quad (48)$$

Here $\tau = \frac{(D)^{\frac{1}{2}}}{\frac{m}{L^2}}$, t is the real time and m is the mass per unit length of the beam and $m = \rho_s A_M + \rho_c A_c$. ρ_s is the density of SMA and ρ_c is the density of epoxy. A_M and A_c are the SMA and epoxy layer cross-section areas, respectively.

The linear parts of Eqs. (47) and (48) are the undamped coupled equations of motion. There are two ways of

obtaining the natural frequencies from these two equations. One is to directly linearize the two equations, which means that the nonlinear part of equations will not have any influence on the system; thus the nonlinear hardening effect due to the large deflection [20] is gone. The other is to locally linearize the two equations at each equilibrium with the different p and T. For the first approach, the governing equations are

$$U_{\tau\tau} + \beta V_{\zeta\zeta\zeta} - \alpha_1 U_{\zeta\zeta} = 0, \tag{49}$$

and

$$V_{\tau\tau} + V_{\zeta\zeta\zeta\zeta} - \beta U_{\zeta\zeta\zeta} - \alpha V_{\zeta\zeta} = 0. \tag{50}$$

For the second approach, let $U = \hat{U} + U'_e, V = \hat{V} + V'_e$ and substitute them into Eqs. (47) and (48), the linearized equations of (47) and (48) around the equilibrium are derived as follows:

$$\hat{U}_{\tau\tau} + \beta\left[1 - \frac{1}{2}(V'_e)^2\right]\hat{V}_{\zeta\zeta\zeta} - \alpha_1\hat{U}_{\zeta\zeta} - (\eta V_e + 2\beta V''_e V'_e)\hat{V}_{\zeta\zeta} - (\eta V''_e + \beta V''_e + \beta V'_e V'''_e)\hat{V}_\zeta = 0, \tag{51}$$

and

$$\hat{V}_{\tau\tau} + \hat{V}_{\zeta\zeta\zeta\zeta} - \beta\hat{U}_{\zeta\zeta\zeta} - \eta V'_e\hat{U}_{\zeta\zeta} - \eta V''_e\hat{U}_\zeta - \left(\alpha + \eta U'_e + \frac{3}{2}\eta V'_e\right)\hat{V}_{\zeta\zeta} - (\eta U''_e + \eta V'_e V''_e)\hat{V}_\zeta = 0. \tag{52}$$

Here U_e, V_e are the equilibria which are solved from Eqs. (24) and (25). Physically, $\hat{U}$ and $\hat{V}$ are the small perturbations from the equilibria of U_e and V_e. For the pinned-pinned beam, $\hat{U}$ and $\hat{V}$ are expanded in sine series. For both equation sets of Eqs. (49), (50) and Eqs. (51), (52), it is the eigenvalue problem to obtain the natural frequencies. For the expansion with n terms, a $2n \times 2n$ matrix is correspondingly obtained either from Eqs. (49) and (50) or from Eqs. (51) and (52). There are n natural frequencies for the transverse displacement V and n natural frequencies for the axial displacement U.

Fig. 18 shows the comparison of the lowest three natural frequencies obtained from Eqs. (49) and (50) when the compression loads are $p = 0$ N and $p = -20{,}000$ N. The beam is symmetric. For the free vibration studied here, all the parameters are taken the same as those in Fig. 7. The increase of compression or ΔT reduces the system stiffness. As shown in Fig. 18, the natural frequencies keep decreasing as the two parameters increase. In Fig. 19, a comparison of the transverse frequencies obtained from Eqs. (49) and (50); Eqs. (51) and (52) with $p = 0$ N is shown. As expected, the transverse frequencies obtained from Eqs. (51) and (52) are always higher than those of (49) and (50) due to the nonlinear hardening effect.

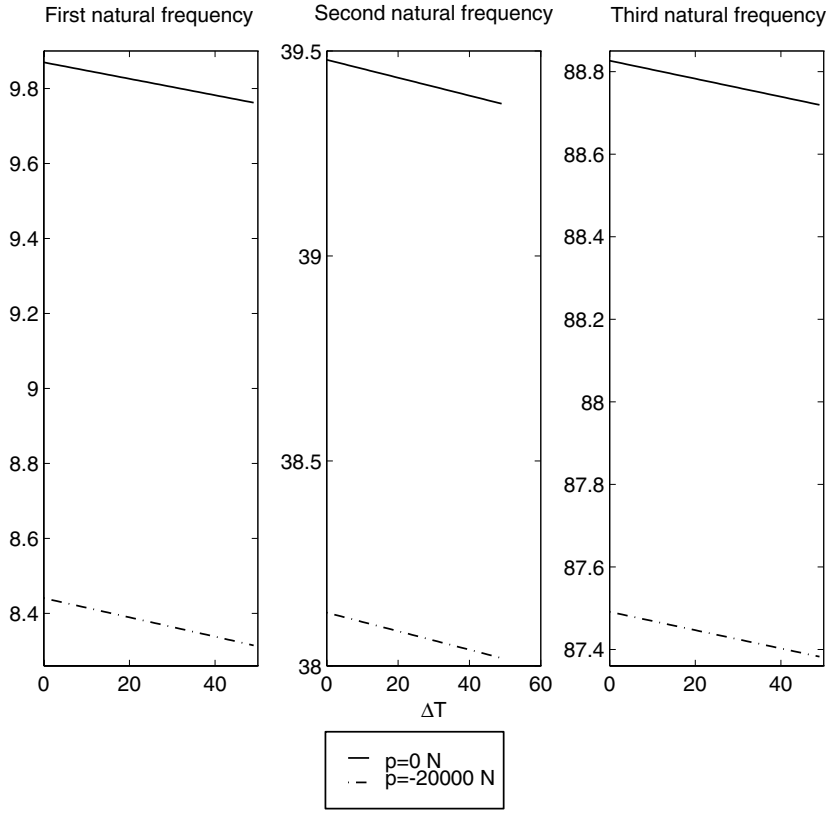

Fig. 18. The comparison of the lowest three natural frequencies of transverse displacement at $p = 0$ N and $p = -20{,}000$ N computed from Eqs. (49) and (50).

5.2. Forced vibration and system response

For the forced vibration, another term, the external work W due to the external shaking force, is added

$$W = \int_0^L f \sin(\omega t)\delta(x - x_0)\,\mathrm{d}x. \tag{53}$$

where f is the external shaking force amplitude and ω is the shaking frequency, t is the real time. $\delta(x - x_0)$ here is Dirac Delta function, x_0 is the shaking force location. Now Hamilton's Principle is applied as follows:

$$\delta(K - U_t + W) = 0. \tag{54}$$

Kinetic energy K and potential energy U_t remain the same as before. In the forced vibration, we focus on the study of the system response as the shaking force changes. FE method is applied here for this study. Young's moduli for SMA and epoxy are taken as $E_s = 20.5 \times 10^{10}$ Pa and $E_c = 53.78 \times 10^{10}$ Pa, respectively. In Fig. 20, three response cases with and without SMA layer and different temperatures are shown. For the two cases with SMA layer in Fig. 20, SMA is not activated, i.e., no recovery stress is induced. For no SMA layer case, the beam has such dimensions of $L = 0.457$ m, $h1 = h2 = 0$ m, $h3 = h4 = 0.0022$ m. For the cases with SMA layer, the parameters are $L = 0.457$ m, $h1 = h2 = 0.0015$ m, $h3 = h4 = 0.0022$ m. $f_{cr} = 155.43$ Hz is the lowest resonance frequency for beam with no SMA layer at temperature $T = 0$ °C. The response in the plot is the largest amplitude of midspan of the beam, which is obtained as the program runs long enough for the system to

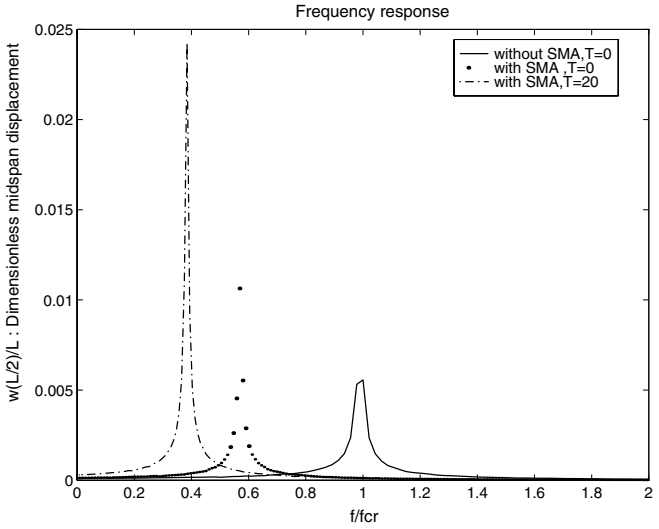

Fig. 20. The frequency response of symmetric beam with and without the SMA layer when $T = 0$ °C and $T = 20$ °C. $f_{cr} = 155.43$ Hz is the resonance frequency for beam with no SMA layer when $T = 0$ °C. For the beam with the SMA layer, the parameters are $L = 0.457$ m, $h_1 = h_2 = 0.0015$ m, $h_3 = h_4 = 0.0022$ m. The external driving force amplitude f is 2.4. At these two temperatures, SMA is not activated.

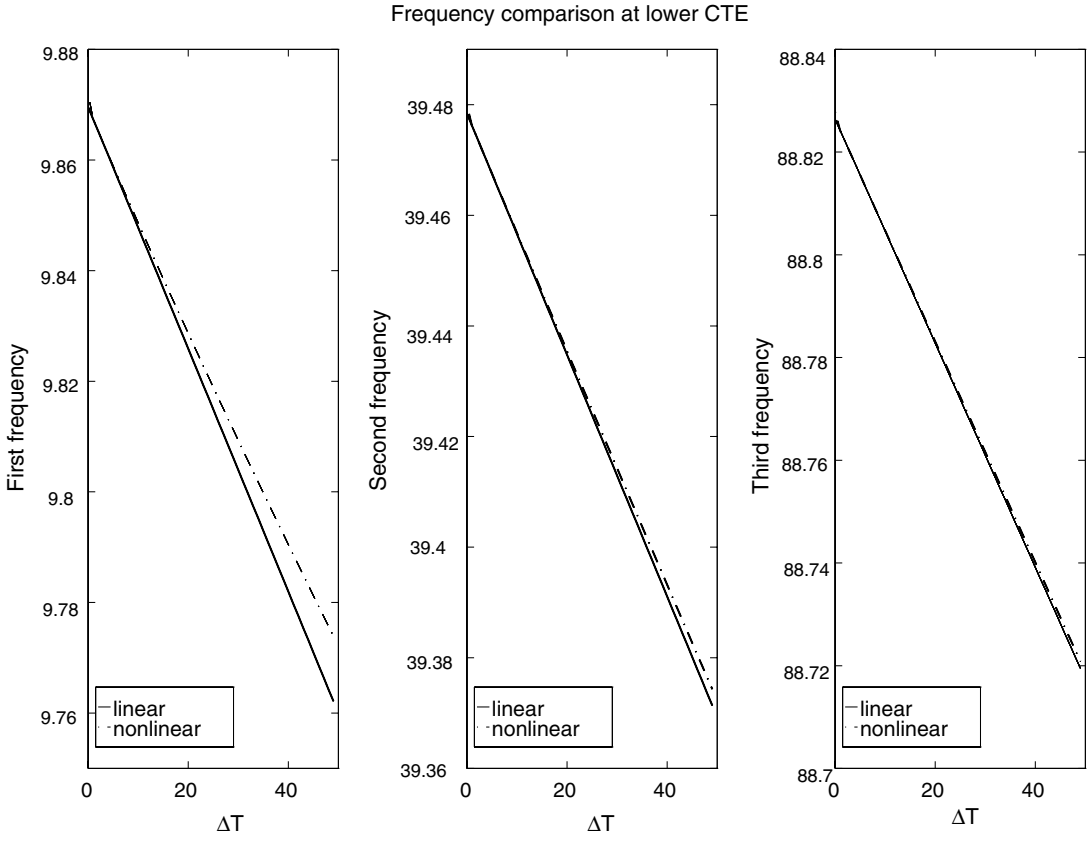

Fig. 19. The comparison of the lowest three transverse natural frequencies at $p = 0$ N computed from Eqs. (49) and (50); Eqs. (51) and (52).

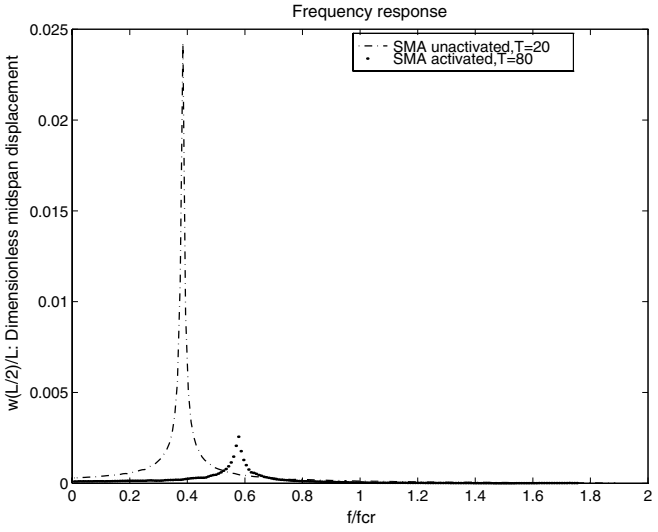

Fig. 21. The frequency response of symmetric beam with the SMA layer at $T = 20$ °C and $T = 80$ °C. $f_{cr} = 155.43$ Hz is the resonance frequency for the beam of same dimensions with no SMA layer at $T = 0$ °C. For the beam with the SMA layer, the parameters are $L = 0.457$ m, $h_1 = h_2 = 0.0015$ m, $h_3 = h_4 = 0.0022$ m. The external driving force amplitude is 2.4. At $T = 80$ °C, the beam is activated.

reach steady state. The shaking amplitude f is taken as 2.4 and x_0 is at the midspan. For the case with no SMA layer, because the epoxy Young's modulus is larger, the response amplitude is smaller and the resonant frequency is higher. And increasing temperature actually increases the compression, which reduces the system stiffness. This response comparison is clearly shown in the two cases with the SMA layer at different temperatures in Fig. 20.

The temperature not only increases the compression but also activates SMA, which generates tensile force. As shown in Fig. 21, the SMA at $T = 80$ °C is activated and the tensile recovery stress surpasses the compressive thermal stress. As a whole, the system is stiffened. So at $T = 80$ °C, the system has higher resonant frequency and lower amplitude than those at $T = 20$ °C. In Fig. 21, it is shown that the beam is symmetric. The related parameters are $L = 0.457$ m, $h1 = h2 = 0.0015$ m, $h3 = h4 = 0.0022$ m. It is worthy pointing out that though there is no damping included, the response amplitude is finite in both Figs. 20 and 21. This is due to the nonlinearity of the governing equations.

6. Summary

This paper gives a comprehensive study on the composite beam with the SMA layer embedded. The study covers the kinematic assumptions, modeling development, equilibrium study, solution discussions (on both linear and nonlinear ones), solution method (FE and Galerkin), buckling, and post-buckling, free vibration and forced vibration. This study uses many numerical and analytical examples to show the influence of modeling and numerical solution method on the computation of the composite beam. Many typical behaviors of composite beam with SMA layer embedded are shown. By analyzing the kinematic assumptions, which are the very start of the mechanics of materials approach to study the composite beam, we show the different kinematic assumption results in different governing equations and solutions. By analyzing the linear and nonlinear solutions, the comparison is shown and the applicability range of linear theory is suggested. We also point out the numerical difficulty of using Galerkin method to study post-buckling behavior by analyzing the expansion terms in Galerkin method. The influence of the other parameters like the SMA layer thickness, shift from the neutral axis, SMA recovery stress on the composite beam equilibrium, post-buckling is also shown. From this comprehensive analysis on the composite beam from the start (the kinematic assumptions) to some typical behaviors (equilibrium, buckling, post-buckling and vibration), many possible reasons causing the difference between the simulation and the real (experimental) data are also explored.

Acknowledgments

Zhang is thankful to the financial supports from both the National Natural Science Foundation of China (NSFC, Grant No. 10502050) and the Scientific Research Foundation for the Returned Overseas Chinese Scholars, State Education Ministry. Zhao is supported by the Distinguished Young Scholar Fund of the National Natural Science Foundation of China (NSFC, Grant No. 10225209), the key project from Chinese Academy of Sciences (Grant No. KJCXSW-L2) and NSFC project (Grant No. 90305020).

Appendix

For the two following equations derived from the kinematic assumption 1, the solution procedure is the same as that of Vinson and Sierakowski [23]

$$Bv_{xxx} - Au_{xx} = 0, \tag{18}$$

and

$$Dv_{xxxx} - Bu_{xxx} = 0. \tag{19}$$

Take one more derivative with respect to x for Eq. (18), and v_{xxxx} and u_{xxx} can be solved by using simple algebra as $v_{xxxx} = 0$ and $u_{xxx} = 0$. Thus u and v have the solution forms of

$$v_{a1} = c_4x^3 + c_5x^2 + c_6x, \tag{31}$$

and

$$u_{a1} = c_1x^2 + c_2x. \tag{32}$$

$c_3 = 0$ because of boundary conditions.

For the solution of linearized equations of equilibrium derived from kinematic assumption 2 or 3, the procedure

is very similar. The linear parts of the governing equations derived from kinematic assumption 2 or 3 are the following

$$\beta V_{\zeta\zeta\zeta} - \alpha_1 U_{\zeta\zeta} = 0, \tag{26}$$

$$V_{\zeta\zeta\zeta\zeta} - \beta U_{\zeta\zeta\zeta} - \alpha V_{\zeta\zeta} = 0. \tag{27}$$

Take one more derivative of Eq. (26), $U_{\zeta\zeta}$ is then solved as $U_{\zeta\zeta\zeta} = \frac{\beta}{\alpha_1} V_{\zeta\zeta\zeta\zeta}$, and substitute this into Eq. (27), we have the following equation:

$$\left(1 - \frac{\beta^2}{\alpha_1}\right) V_{\zeta\zeta\zeta\zeta} - \alpha V_{\zeta\zeta} = 0.$$

The characteristic equation for the equation above is

$$\lambda^2 \left[\left(1 - \frac{\beta^2}{\alpha_1}\right)\lambda^2 - \alpha\right] = 0.$$

Now it is clear for different $\gamma = \frac{-\alpha}{1-\frac{\beta^2}{\alpha_1}}$, the solution forms change accordingly in Eqs. (33), (34) (35), and (36).

References

[1] Buehler WJ, Wiley RC. US patent 3,174,851: nickel-based alloys, 1965.
[2] Tanaka K. A thermo-mechanical sketch of shape memory effect: one dimensional tensile behaviour. Res Mech 1986;8:251–63.
[3] Tanaka K, Nagaki S. A thermomechanical description of materials with internal variables in the process of phase transformation. Ingenieur-Archiv 1982;51:287–99.
[4] Liang C, Rogers CA. One dimensional thermomechanical constitutive relations for shape memory material. J Intell Mater Struct 1990;20:207–34.
[5] Rogers CA, Liang C. Behaviour of shape memory alloy reinforced composite plates, Part I: model of formulations and control concepts. In: Proceedings of the 30th structures, structural dynamics and materials conference, Mobile, AL, 1989. p. 2011–7.
[6] Xue DY, Mei C. A study of the application of shape memory alloy in panel flutter control. In: Proceedings of 5th international conference on recent advances in structural dynamics 1994. p. 412–22.
[7] Cross WB, Kariotis AH, Stimler FJ. Nitinol characterization study. 1969. NASA CR-1433.
[8] Jackson CM, Wagner HJ, Wasilewski RJ. 55-Nitinol the alloy with a memory: its physical metallurgy, properties and applications. 1972. NASA SP-5110.
[9] Turner TL. A new thermoelastic model for analysis of shape memory alloy hybrid composites. J Intell Mater Struct 2000;11:382–94.
[10] Baz A, Ro J. Thermo-dynamic characteristics of NITINOL-reinforced composite beams. Compos Eng 1992;2:527–42.
[11] Epps J, Chandra R. Shape memory alloy actuation for tuning of composite beams. Smart Mater Struct 1997;20:251–6.
[12] Zhang Y, Zhao YP. A discussion on modeling shape memory alloy embedded in a composite as axial force and elastic foundation, Mater Des 2006 (in press).
[13] Rogers CA. Active vibration and structural acoustic control of shape memory alloy hybrid composite: experimental results. J Acoust Soc Am 1990;88:2803–11.
[14] Baz A, Imam K, McCoy J. Active vibration control of flexible beam using shape memory actuators. J Sound Vib 1990;140:437–56.
[15] Chaudhry Z, Rogers CA. Bending and shape control of beams using SMA actuators. J Intell Syst Struct 1991;2:581–602.
[16] Hearn EJ. Mechanics of materials. 2nd ed. Oxford: Pergamon Press; 1985.
[17] Beer F, Johnston R, DeWolf J. Mechanics of materials. 3rd ed. New York: The McGraw-Hill Companies; 2001.
[18] Christensen RM. Mechanics of composite materials. Malabar, FL: Krieger Publishing Company; 1991.
[19] Bowling NE. Mechanical behavior of materials: engineering methods for deformation, fracture, and fatigue. 2nd ed. New Jersey: Prentice-Hall; 1999.
[20] Nayfeh AH, Mook DT. Nonlinear oscillations. New York: Wiley; 1979.
[21] Thurman AL, Mote CD. Free, periodic, nonlinear oscillation of an axially moving strip. J Appl Mech 1969;36:83–91.
[22] Thurman AL, Mote CD. Nonlinear oscillation of a cylinder containing a flowing fluid. J Eng Ind 1969;91:1147–55.
[23] Vinson JR, Sierakowski RL. The behavior of structures composed of composite materials. Kluwer Academic Publishers; 1987.
[24] King JL. The free transverse vibrations of anisotropic beams. J Sound Vib 1985;98:575–85.
[25] Meirovitch L. Analytical methods in vibrations. New York: Macmillan Publishing Co. Inc.; 1967.
[26] Meirovitch L. Computational methods in structural dynamics. Rockville, MD: Sijthoff & Noordhoff; 1980.
[27] Timoshenko S. Theory of elastic stability. Engineering societies monographs. 1st ed. New York: The McGraw-Hill Companies; 1936.
[28] Chajes A. Principles of structural stability theory. Englewood Cliffs, NJ: Prentice-Hall, Inc.; 1974.
[29] Banerjee JR. Explicit analytical expressions for frequency equation and mode shapes of composite beams. Int J Solids Struct 2001;38:2415–26.
[30] Hughes TJR. The finite element method, linear static and dynamic finite element analysis. Englewood Cliffs, NJ: Prentice-Hall; 1987.